



Multifunctional Material Systems for Reconfigurable Antennas

Gregory Huff
TEXAS ENGINEERING EXPERIMENT STATION COLLEGE STATION

01/05/2016
Final Report

DISTRIBUTION A: Distribution approved for public release.

Air Force Research Laboratory
AF Office Of Scientific Research (AFOSR)/ RTB2
Arlington, Virginia 22203
Air Force Materiel Command

REPORT DOCUMENTATION PAGE					<i>Form Approved</i> OMB No. 0704-0188	
<p>The public reporting burden for this collection of information is estimated to average 1 hour per response, including the time for reviewing instructions, searching existing data sources, gathering and maintaining the data needed, and completing and reviewing the collection of information. Send comments regarding this burden estimate or any other aspect of this collection of information, including suggestions for reducing the burden, to Department of Defense, Washington Headquarters Services, Directorate for Information Operations and Reports (0704-0188), 1215 Jefferson Davis Highway, Suite 1204, Arlington, VA 22202-4302. Respondents should be aware that notwithstanding any other provision of law, no person shall be subject to any penalty for failing to comply with a collection of information if it does not display a currently valid OMB control number.</p> <p>PLEASE DO NOT RETURN YOUR FORM TO THE ABOVE ADDRESS.</p>						
1. REPORT DATE (DD-MM-YYYY) 12/17/2015		2. REPORT TYPE Final			3. DATES COVERED (From - To) 04/1/2012 - 09/30/2015	
4. TITLE AND SUBTITLE Multifunctional Material Systems for Reconfigurable Antennas in Superconfigurable Structures				5a. CONTRACT NUMBER FA9550-12-1-0090		
				5b. GRANT NUMBER FA9550-12-1-0090		
				5c. PROGRAM ELEMENT NUMBER 		
6. AUTHOR(S) Dr. Gregory H. Huff				5d. PROJECT NUMBER 		
				5e. TASK NUMBER 		
				5f. WORK UNIT NUMBER 		
7. PERFORMING ORGANIZATION NAME(S) AND ADDRESS(ES) Texas Engineering Experiment Station 1470 William D Fitch Parkway College Station, TX 77845-4645					8. PERFORMING ORGANIZATION REPORT NUMBER C12-00550	
9. SPONSORING/MONITORING AGENCY NAME(S) AND ADDRESS(ES) Air Force Office of Scientific Research 875 N. Randolph St. Room 3112 Arlington, VA 22203					10. SPONSOR/MONITOR'S ACRONYM(S) USAF/AFRL	
					11. SPONSOR/MONITOR'S REPORT NUMBER(S) 	
12. DISTRIBUTION/AVAILABILITY STATEMENT Approved for public release, distribution unlimited						
13. SUPPLEMENTARY NOTES						
14. ABSTRACT The overarching goal of this project is to pursue multidisciplinary engineering research objectives related to the analysis, design, operation, and integration of superconfigurable antenna systems enabled by fluidic dispersions of nanoparticles and multifunctional composites. This final report summarizes major research accomplishments and other highlights from this research program.						
15. SUBJECT TERMS Reconfigurable antennas, nanocomposites, dispersions, superconfigurable systems						
16. SECURITY CLASSIFICATION OF:			17. LIMITATION OF ABSTRACT UU	18. NUMBER OF PAGES	19a. NAME OF RESPONSIBLE PERSON	
a. REPORT U	b. ABSTRACT U	c. THIS PAGE U			19b. TELEPHONE NUMBER (Include area code)	

INSTRUCTIONS FOR COMPLETING SF 298

1. REPORT DATE. Full publication date, including day, month, if available. Must cite at least the year and be Year 2000 compliant, e.g. 30-06-1998; xx-06-1998; xx-xx-1998.

2. REPORT TYPE. State the type of report, such as final, technical, interim, memorandum, master's thesis, progress, quarterly, research, special, group study, etc.

3. DATE COVERED. Indicate the time during which the work was performed and the report was written, e.g., Jun 1997 - Jun 1998; 1-10 Jun 1996; May - Nov 1998; Nov 1998.

4. TITLE. Enter title and subtitle with volume number and part number, if applicable. On classified documents, enter the title classification in parentheses.

5a. CONTRACT NUMBER. Enter all contract numbers as they appear in the report, e.g. F33315-86-C-5169.

5b. GRANT NUMBER. Enter all grant numbers as they appear in the report. e.g. AFOSR-82-1234.

5c. PROGRAM ELEMENT NUMBER. Enter all program element numbers as they appear in the report, e.g. 61101A.

5e. TASK NUMBER. Enter all task numbers as they appear in the report, e.g. 05; RF0330201; T4112.

5f. WORK UNIT NUMBER. Enter all work unit numbers as they appear in the report, e.g. 001; AFAPL30480105.

6. AUTHOR(S). Enter name(s) of person(s) responsible for writing the report, performing the research, or credited with the content of the report. The form of entry is the last name, first name, middle initial, and additional qualifiers separated by commas, e.g. Smith, Richard, J, Jr.

7. PERFORMING ORGANIZATION NAME(S) AND ADDRESS(ES). Self-explanatory.

8. PERFORMING ORGANIZATION REPORT NUMBER. Enter all unique alphanumeric report numbers assigned by the performing organization, e.g. BRL-1234; AFWL-TR-85-4017-Vol-21-PT-2.

9. SPONSORING/MONITORING AGENCY NAME(S) AND ADDRESS(ES). Enter the name and address of the organization(s) financially responsible for and monitoring the work.

10. SPONSOR/MONITOR'S ACRONYM(S). Enter, if available, e.g. BRL, ARDEC, NADC.

11. SPONSOR/MONITOR'S REPORT NUMBER(S). Enter report number as assigned by the sponsoring/monitoring agency, if available, e.g. BRL-TR-829; -215.

12. DISTRIBUTION/AVAILABILITY STATEMENT. Use agency-mandated availability statements to indicate the public availability or distribution limitations of the report. If additional limitations/ restrictions or special markings are indicated, follow agency authorization procedures, e.g. RD/FRD, PROPIN, ITAR, etc. Include copyright information.

13. SUPPLEMENTARY NOTES. Enter information not included elsewhere such as: prepared in cooperation with; translation of; report supersedes; old edition number, etc.

14. ABSTRACT. A brief (approximately 200 words) factual summary of the most significant information.

15. SUBJECT TERMS. Key words or phrases identifying major concepts in the report.

16. SECURITY CLASSIFICATION. Enter security classification in accordance with security classification regulations, e.g. U, C, S, etc. If this form contains classified information, stamp classification level on the top and bottom of this page.

17. LIMITATION OF ABSTRACT. This block must be completed to assign a distribution limitation to the abstract. Enter UU (Unclassified Unlimited) or SAR (Same as Report). An entry in this block is necessary if the abstract is to be limited.

Report Type: Final Progress Report
Grant Number: FA9550-12-1-0090
Program Manager: Dr. Byung-Lip Lee
Proposal Title: Multifunctional Material Systems for Reconfigurable Antennas in Superconfigurable Structures
Principle Investigators: Gregory H. Huff, Texas A&M University
Michael A. Bevan, Johns Hopkins University
Zoubeida Ounaies, Pennsylvania State University
Performance Period: 01-APR-2012 to 30-SEP-2015

A. Project Summary

The overarching goal of this project is to pursue multidisciplinary engineering research objectives related to the analysis, design, operation, and integration of superconfigurable antenna systems enabled by fluidic dispersions of nanoparticles and multifunctional composites. A multi-scale approach focusing on a range of carefully targeted experimental observations, numerical simulations, and analytical modeling techniques are being used to accomplish the individual tasks associated with this objective. This broadly-defined scope of activities also serves as a connective mechanism between fundamental physical behavior and intrinsic properties to paradigms for dynamic control at the particle level to engineering design concepts and application spaces. Several system-level demonstration vehicles are examined in this process, which are intended to act as a pathway for the transition of these advancements into relevant technologies.

Activities in this project include the fabrication and evaluation of new fluidic-based material systems, integrative and adaptive control techniques, and the application of these dynamic systems to engineer novel superconfigurable antenna systems. This includes reconfiguration mechanisms (switches, reactive loads, and filters) and reconfigurable antennas (resonant and traveling wave) are being developed to study the interaction of these materials systems at the application-scale to facilitate changes in frequency selectivity, directional radiation characteristics, and thermal behavior in an automated deformable antenna test-bed. Microstrip and stripline topologies will be focused on for this project to ensure interoperability of new technologies since these topologies are readily integrated into existing systems. These will be engineered around the common operational objective of enabling advanced sensing (radar) and wireless (communication) technologies in a collection of frequency bands of strategic interest to the Air Force and other DoD branches. This will include UHF (0.3-3 GHz), S-Band (2-4 GHz), and X-band (8-12 GHz), but analysis and experimentation will be performed on high performing technologies up to the PI's instrumentation limit of 70 GHz (into V-band) to explore emerging design spaces.

The research objectives associated with this project are summarized in the following section in numbered lists 1-4; we have included goals and expected outcomes from the proposal, and the specific challenges for each facet of this project are delineated in lower case roman numerals (i, ii, etc.) for distinction. Major accomplishments and project highlights are included with each sub-section to provide a comprehensive but brief overview of project activities.

B. Project Accomplishments

1. Synthesis and Customization of High Aspect Ratio Nanoparticles

- **Goal:** The goals of this objective are to develop of a synthesis process for obtaining high yields of currently unobtainable high aspect ratio particles and characterize their electromagnetic properties at high frequencies using multi-scale models and experimental observations
- **Expected outcome:** The expected outcomes of this objective are design-driven synthesis and processing steps for custom-shaped electrically-dense nanoparticles and advanced mixing formula which accurately capture the properties of these particles in both fluidic dispersions and composites

i. Provide increased yields of high aspect ratio ferroelectric nanoparticles

Progress in materials synthesis and characterization was focused on three tasks: 1) using a modified hydrothermal technique that led to more robust and tunable results; 2) further improving the process to generate higher and more repeatable yields; 3) establishing a process for functionalization of nanoparticle surface to provide multi-layer coatings to tune electric field guided manipulation (Fig. 1).

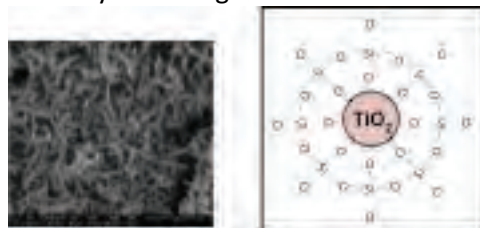


Fig. 1 LEFT: Example of high aspect ratio ferroelectric particles synthesized using hydrothermal method. RIGHT: Functionalization of dielectric particle to tune electrokinetic interactions.

The lack of commercially available nanoparticles with high dielectric strength and low losses created the critical need to synthesize high aspect ratio nanoparticles with the required ability to provide high fidelity control of their distribution and orientation in composites. As a result, our efforts focused on the design-driven synthesis and processing steps for custom-shaped electrically-dense nanoparticles to facilitate high-yields of high dielectric mixed-oxide ferroelectric anisotropic particles. We have shown in the previous report a repeatable robust method of synthesizing high aspect ratio barium titanate (BTO) nanowires. By controlling the amount of surfactant added, aspect ratio of ferroelectric BTO varied between ~ 5 to ~ 10 . We also undertook the synthesis of other custom nanoparticles; for example, we were successful in synthesizing titania nanoparticles to various shapes and aspect ratios, with the goal of embedding them in composites to fabricate substrates with tailorable EM properties.

We have also carried out the development of judicious coatings of above high aspect ratio high dielectric particles to add more control over assembly of these particles in the presence of electric field and hence, enable tuning of the final microstructure in fluids and composites through electric-field-guided manipulation (Fig. 2). The presence of judicious surface modification of mixed oxide particles reduces dielectric contrast between said-particles and the dielectric medium (whether fluid or polymer). Regulation of dielectric contrast through surface chemistry leads to better control of dispersion, distribution and electric field manipulation. Some of that is discussed in the next sections. Both developing the ability to synthesize custom particles then modify them through chemistry provide insight into the fundamental relationships between synthesis, morphology, and constitutive parameters and assists in the development of anisotropic composites and microfluidic-based antenna. One important result that emerged this past year is that the synthesis and coating of high aspect ratio nanoparticles can improve electric field-mediation with prescribed dielectric gradients, resulting in the ability to capture and fully exploit the electromagnetic properties of custom high aspect ratio nanoparticles at multiple length scales in both fluidic dispersions and composites.

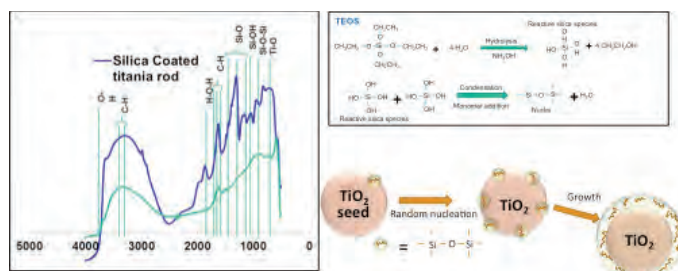


Fig. 2 (Left) FTIR characterization of functionalized high aspect ratio titania confirms presence of silica coating. (Right) Scheme for surface modification of titania particle to tune electrokinetic response.

Hydrothermal synthesis has been considered in this project for its ability to produce increased yields of high aspect ratio BaTiO₃ (BT) particles since it has been widely used for the preparation of nanostructured materials and shown to be effective in synthesis of BT in the form of nanowires, nanorods, and nanotubes. Despite the recent widespread use of this technique, consistently obtaining high aspect ratio BT in a pure ferroelectric (high permittivity) phase remains elusive. In a previous report, we demonstrated successful use of hydrothermal technique to synthesize low aspect ratio BT and we showed evidence of tetragonal phase (with a broader peak at $2\theta = 45^\circ$ - 46° range; see Fig. 3). In this reporting period, we follow a modified hydrothermal approach with the focus of chemically inducing the ferroelectric phase while encouraging and maintaining a high aspect ratio, rapidly and in a scalable fashion. Fig. 3 illustrates this new modified approach. FE-SEM and XRD were used to characterize the as-prepared products.

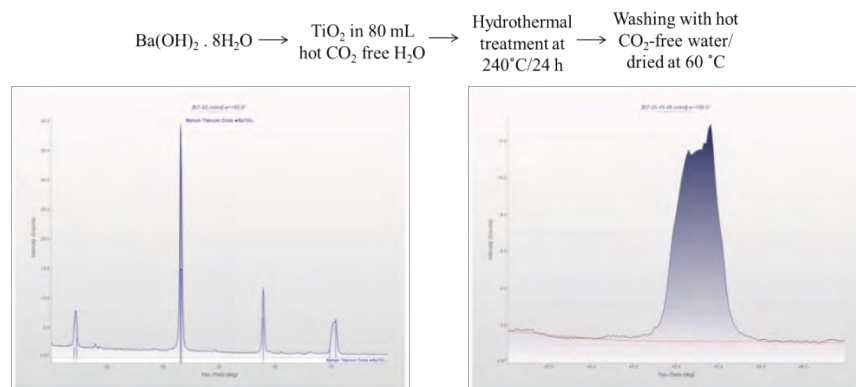


Fig. 3 (top) Outline of current hydrothermal process used to synthesize BaTiO₃ nanowires, (bottom left) X-Ray diffraction (XRD) results for one of the samples using this process to illustrate purity, and (bottom right) the increased scan resolution in the $2\theta = 45^\circ$ - 46° range indicating the formation of the desired tetragonal crystalline structure (through the split peaks observed in this range).

In this modified hydrothermal approach, precursors of Ba and Ti were modified and a surfactant is introduced. Specifically, the following chemicals were used for synthesis of BT nanowires: titanium tetrachloride (TiCl₄), barium chloride (BaCl₂), ethylene glycol (as surfactant) and sodium hydroxide (NaOH) as the base; all chemicals were purchased from Alfa Company. Specific amounts and steps are shown in Fig. 4 (left). After cooling in the hydrothermal reactor, the synthesized BT was separated by centrifugation and washed with hot DI water 5 times and acetic acid 3 times to remove impurities, mostly present in the form of BaCO₃. Inspection of Fig. 4 (right) reveals that all the diffraction peaks can be assigned to the BT crystal structure without any impurity or byproducts. More importantly, clear splitting of diffraction peak at $2\theta=45^\circ$, related to (002) and (202), further reveals that tetragonal structure is the main phase in BT. In addition, splitting of peak at $2\theta=22^\circ$ is also observed with this modified approach, further cementing the fact that the dominating phase is tetragonal.

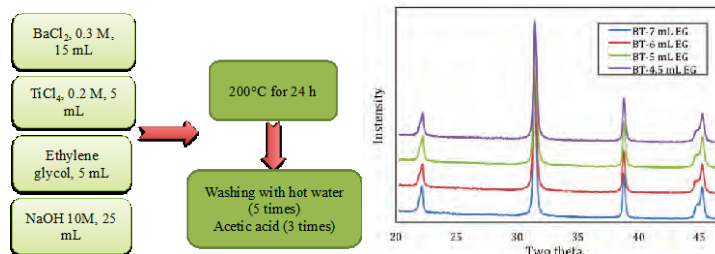


Fig. 4 (Left) Modified hydrothermal technique utilizes new precursors for Ba and Ti and incorporate use of ethylene glycol and NaOH to control the pH of the reaction. (Right) X-Ray diffraction (XRD) results for a series of BT synthesized with increasing amounts of ethylene glycol. XRD illustrates the purity of BT, and the obviously split peak at 45° proves that the phase is the desired tetragonal crystalline structure.

Our experiments indicate that the morphology of BT depends on the hydrothermal conditions (temperature/time) and amount of surfactant (EG). In particular, reaction temperature and time affected the amount of tetragonal phase while the surfactant EG had an important influence on aspect ratio and shape in general. A series of reaction were carried out to understand effect of EG on the shape of particles in the system. Fig. 4 (left) shows x-ray diffraction of BaTiO₃ using different amounts of EG. Again, in all cases, all the diffraction peaks are assigned to tetragonal BaTiO₃. No characteristic peaks of other impurities were observed, indicating that the entire product has high crystallinity and purity. Fig. 5 shows SEM images of BT nanowires under different amount of EG. The aspect ratio of particles changed by changing the EG amount, which confirms that EG had tremendous effect on morphology. When amount of EG is 4.5 mL, widths of BT varied from 70 nm to 225 nm, while their lengths ranged from 340 nm to 1.5 μm whereas BT synthesized with 7 mL EG were in average narrower but longer, resulting in a higher aspect ratio (Fig. 5 a and c). The aspect ratios of prepared samples with different amount of EG are summarized in Table 1.

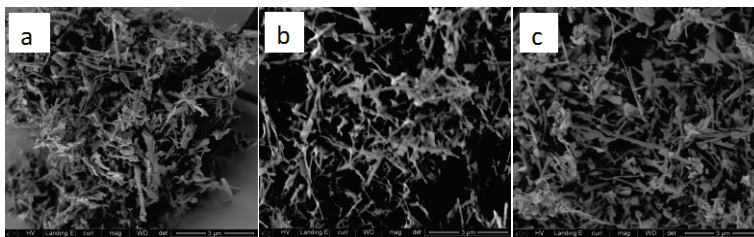


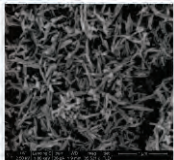
Fig. 5 SEM images of BT showing impact of EG on morphology: a) 4.5 mL, b) 6 mL and c) 7 mL EG

Table 1. Effect of different amounts of EG on the aspect ratios of prepared BaTiO₃ nanowires.

EG (mL)	Width (nm)	Length (nm)	Aspect ratio	SEM
4.5	140	715	5.2	
5	152	807	5.4	
6	135	1194	8.9	
7	177	1400	9.5	

The synthesis of other custom nanoparticles was also explored in this project; for example, there was success in synthesizing titania nanoparticles to various shapes and aspect ratios, with the goal of embedding them in composites to fabricate substrates with tailorable EM properties. Table 2 lists the parameters used in synthesizing titania nanowires in the rutile phase ($\epsilon_r \sim 100\text{-}170$) at low temperatures using the hydrothermal route. Fig. 6 is XRD which confirms the phase and purity of titania.

Table 2. Processing parameters and precursors for the synthesis of rutile pure titania nanowires.

Sample	Precursors	Time	Temp.	Shape	Structure	SEM
W-1	$\text{TiCl}_3, \text{H}_2\text{O}$	72 h	100 °C	nanowires	Rutile	

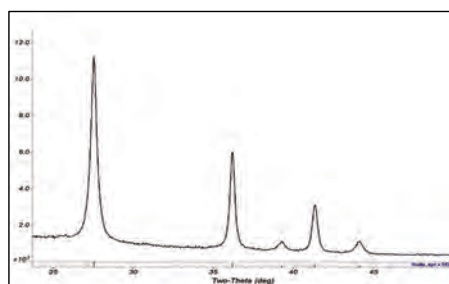


Fig. 6 SEM Pure Rutile structure of TiO_2 confirmed X-ray diffraction analysis

As stated above, our main objective in this task is to design and synthesize custom-shaped electrically-dense nanoparticles and realize desirable EM properties in both fluidic dispersions and composites. For that reason, in addition to synthesizing high permittivity particles, our focus in the past year has been on surface modification and functionalization to tailor dispersion and interfacial interactions in fluidic and prepolymer media (Fig. 7).

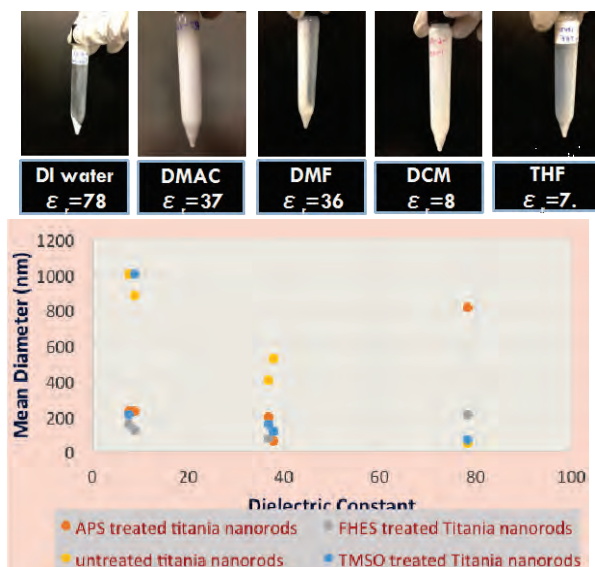


Fig. 7 Next steps in dispersing and manipulating nanoparticles include determining what the best solvent and best functionalization is for treated nanorods (top) and what the combination of colloidal dispersions, functionalization and solvents is best for dispersion, interaction, and dielectric behavior.

TiO₂ rutile nanoparticle (TRNP) can be manipulated by modifying the surface with different silane functional group and hence the compatibility and dispersion in different organic solvents can be improved. In this past year, the dispersion behavior of TRNPs having surfaces modified with APS, FHES and TMSO silane coupling agents in various organic solvents has been studied. The dispersion quality is judged by Dynamic Light Scattering (DLS) measurements and by visual inspection after centrifuging the suspensions. The hydrodynamic mean diameter of NPs is found to vary with the variation of solvents. When the solubility parameters of solvent and surface modified nanoparticle (SMNP) are close to each other the particles tend to disperse at their initial size and there is less chance for agglomeration. It is found that modification of surface of the untreated TRNPs by different silane coupling agent changes the surface behavior dramatically. While the untreated NPs tend to disperse well in polar aprotic solvents, APS silane modification of surface leads the NPs to disperse only in polar protic solvent. TMSO silane modification leads NPs to disperse both in polar protic and aprotic solvents which have high dielectric constant. Interestingly, the FHES silane modified TRNP disperse well in most of the solvents except very high polar and nonpolar solvent.

For each treated particle the optimum dispersion point in which best dispersion is achieved is also calculated. It is found that, while for the untreated particle the dispersion force is the dominant force, APS treated NP shows an increase in hydrogen bonding contribution relative to dispersion force contribution to total solubility. The TMSO treated NP shows good dispersion in a different solubility zone where dispersion and polar forces are the main contributor to total solubility. FHES treated NP shows an increase and shift in solubility zone where many solvents shows good dispersion. In summary, while the untreated nanoparticles tend to disperse well in polar aprotic solvents, APS silane modification of surface leads the NPs to disperse only in polar protic solvent. TMSO silane modification leads NPs to disperse both in polar protic and aprotic solvents only those have high dielectric constant. Interestingly, the FHES silane modified TRNP disperse well in most of the solvents except highly polar and nonpolar solvents. This study is significant for *Objective 2: Control and Mediation of Nanoparticles* since nanoparticle-nanoparticle interactions and nanoparticle-medium interphase become significant.

ii. Link processing steps to particle morphology and high frequency EM properties

This project has investigated electric field mediated manipulation of nanoparticles in 1) non-aqueous media (i.e., silicone oil) and 2) in prepolymer solutions (epoxies and vinyl polymer solutions). The goal of 1) is to determine parameters for alignment and impact on in-situ dielectrics, while the goal of 2) is to design composite substrates with tailored EM properties resulting from texturing of high aspect ratio nanoparticles. By investigating effect of the processing parameters, such as electric field magnitude, frequency, duration, particle chemistry, dielectric medium type, we plan to advance the design-driven synthesis and processing steps for custom-shaped electrically-dense nanoparticles. Fig. 8 presents a snapshot of results pertaining to the electric field manipulation of BTO nanowires in a dielectric fluid or prepolymer, and impact of said-alignment on effective dielectric permittivity. The goals from this study are to 1) integrate the electromagnetically-mediated control of nanoparticles into electrode topologies that are native to high frequency design for reconfigurable antennas, and 2) develop locally-controlled anisotropy in electronically tunable composites. The first goal enables us to advance the task on design of reconfigurable antennas by enabling reconfiguration mechanisms where the functionality is derived from dynamic particle interactions as a result of applied electric field. The second goal makes possible structured substrate composites which can provide advanced control of high frequency wave impedance and propagation velocity owing to the controlled distribution of high dielectric constant high aspect ratio particles.



Fig. 8 LEFT: Electric field drive chaining of high aspect ratio, ferroelectric BTO in dielectric prepolymer; and example of planar electrodes and resulting structured configuration of particles in epoxy. RIGHT: Impact of electric field duration on effective dielectric permittivity of BTO-modified dielectric suspensions.

With regards to texturing in non-aqueous media, the BaTiO_3 nanowires were dispersed in DMF and oil by mechanical stirring and bath sonication. A summary of OM images of BT nanowire alignment in the random case and under different external applied electric fields are shown in Fig. 9 and Fig. 10 (note that the BT loading in both cases is low, less than 0.5 wt%). In Fig. 9, the external AC electric fields had varying magnitudes at the same frequency of 1 kHz. At 500 V/mm no visible chains formed within the 60 minutes of the application of electric field. At 1000 and 2000 V/mm, after 15 minutes the particles started forming chains parallel to the applied electric field. One hour after the application, thin parallel chains were formed between the electrodes. The alignment became stable after 1 h application of the electric field.

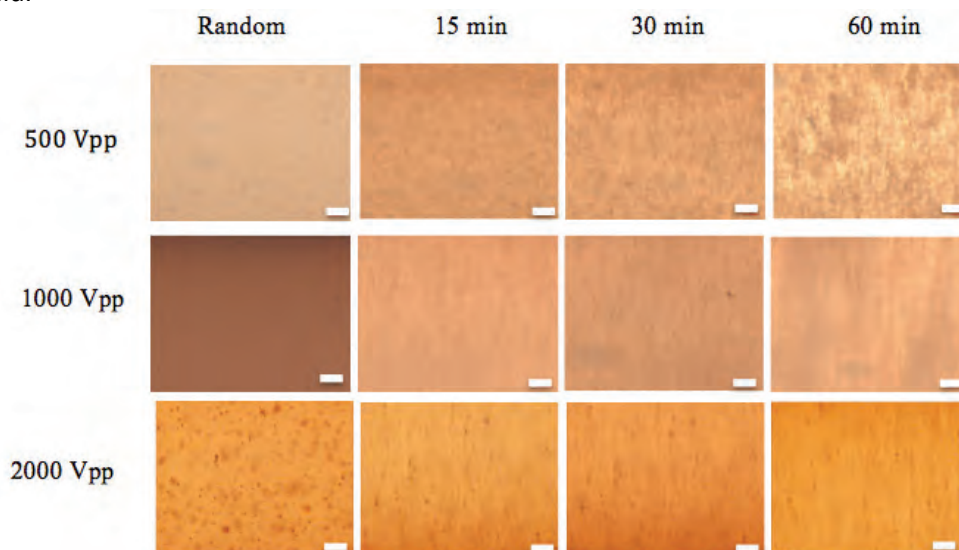


Fig. 9 Optical microscopy images of 0.5 wt% BaTiO_3 nanowires-oil system under an applied electric field of 1 kHz, different magnitudes and different time intervals. The scale bar is 50 μm .

In Fig. 10, the external AC electric fields had the same frequency of 10 kHz, but the magnitudes of the applied fields varied from 500, 1000 to 2000 V/mm. As the frequency of the applied field increased to 10 Hz, no obvious chains formed within the 60 minutes of the application of electric field. From the experimental results, the chain formation of the nanoparticles dispersion was dependent on the frequency applied electric field, and duration of the applied electric field. In-situ dielectric characterization of nanowires aligned in a dielectric medium (silicone oil) confirms impact of texturing on dielectric properties, specifically, Fig. 11 illustrates impact of alignment parameters and aspect ratio on final dielectric properties. One conclusion is that higher aspect ratio nanowires have a higher impact on effective dielectric constant after alignment.

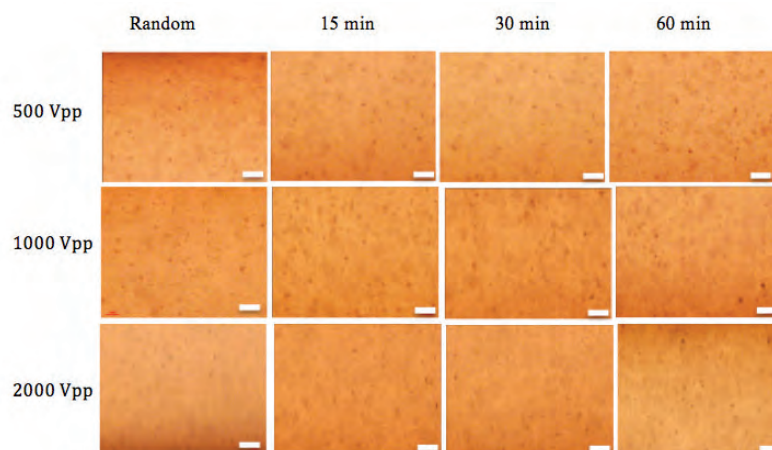


Fig. 10 Optical microscopy images of 0.5 wt% BaTiO₃ nanowires-oil system under an applied electric field of 10 kHz, different magnitudes and different time intervals. The scale bar is 50 μ m.

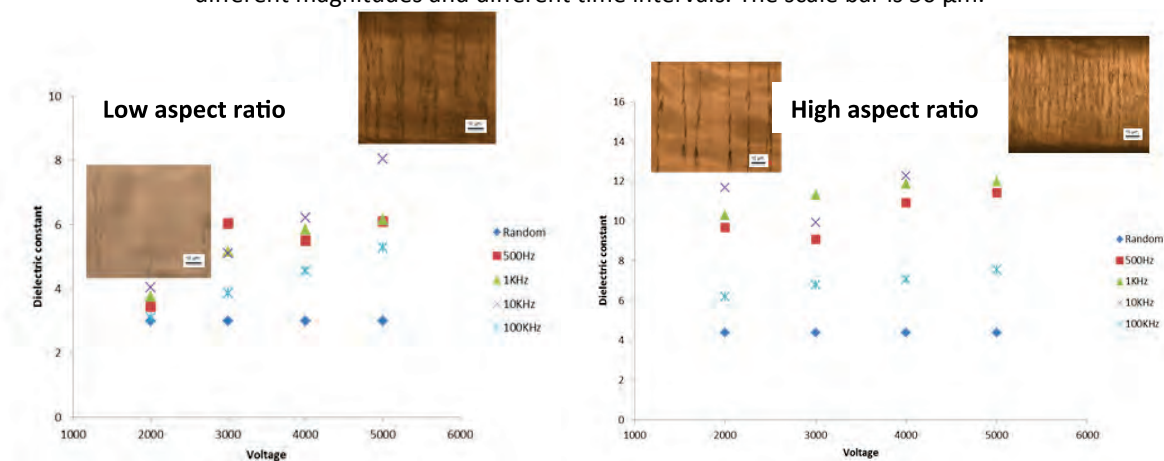


Fig. 11 Impact of orientation and aspect ratio on EM properties

This project has also focused on extending microscopy techniques and analysis methods to measure interactions of anisotropic particles in non-aqueous and pre-polymer media. These build on previous studies of spherical particles in aqueous and non-aqueous media. Work in this project has shown (Fig. 12) how optical microscopy measurements of single particle interacting with electric fields as a function of frequency and amplitude can be used to extract the complete dielectric spectrum, $\epsilon(\omega)$, of the particles and medium including dielectric constants and conductivities. After measuring single particles, we have also shown how particles at different concentrations and configurations can be measured in the same experimental geometry to connect single particle properties to emergent ensemble particle properties. In short, the single particle properties are entered into an inverse Monte Carlo analysis that adjusts the ensemble properties in an iterative manner until they match the measurements. As a result, the dispersion dielectric spectrum is obtained without a mixing rule. Most recently, we have adapted this to measurements of anisotropic particles important to the current project by monitoring anisotropic particle orientation in addition to position (for single particles) and concentration and configuration (in many particle systems). These methods/analyses have been adapted to measure interactions of anisotropic particles in non-aqueous and prepolymer media by taking into account low dielectric constants and conductivities as well as orientational ordering effects in oligomeric prepolymers.

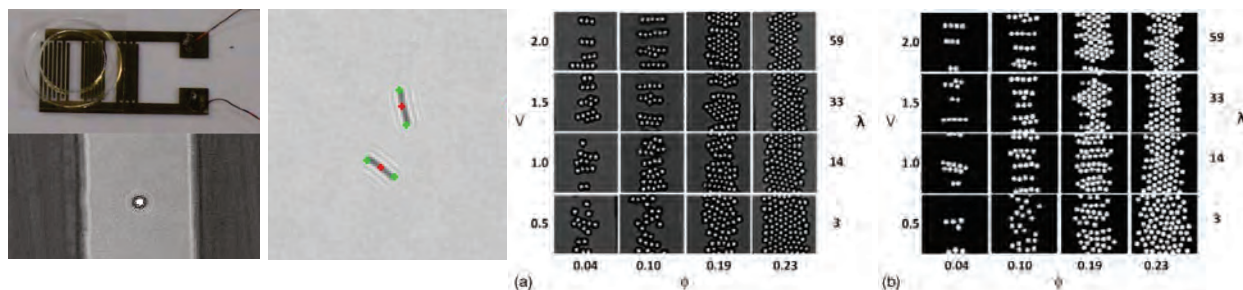


Fig. 12 (far left) Schematics related to single particle measurement configuration. (middle left) Center of mass and orientation tracking of $2\mu\text{m}$ gold nanorods in parallel electrode geometry. (middle right) video microscopy images of equilibrated colloids within electrode gap as a function of field amplitude at 1MHz. (far right) Monte Carlo simulated configurations from potentials obtained via inverse analysis to give concentration and configuration dependent dielectric spectrum without mixing rule.

iii. Develop rigorous statistical models for particles systems with polydisperse aspect ratios

A number of activities focused on the development of advanced physical models and mixing formula for predicting effective medium properties of nanoparticle dispersions at high frequencies. This includes the study of representative volume element (RVE) simulations to develop baseline performance metrics and explore some of the basic physical mechanisms that lead to deviations from Maxwell-Garnett and other mixing formula/rules (which typically occur at higher frequencies and volume fractions). Fig. 13 shows one of the quasi-static simulations obtained using COMSOL for a face-centered cubic (BCC) unit cell and the effective permittivity obtained from sweeping the spherical particle radii of the elements in this unit cell. This is plotted against the Maxwell-Garnett mixing formula (labeled “M-G Rule”), and deviations can be seen that become pronounced above a volume fraction of 60%. There has been a substantial amount of prior work in this area (including RVE simulations and analytical work), but modeling these structured RVEs provides a pathway to benchmark the basic capabilities of the numerical simulations at high frequencies. More importantly, this provides a pathway to integrate with low-frequency models and experimentally-obtained values using energy landscape calculations in this work for high aspect ratio particles (both known and desired permittivity and conductivity properties).

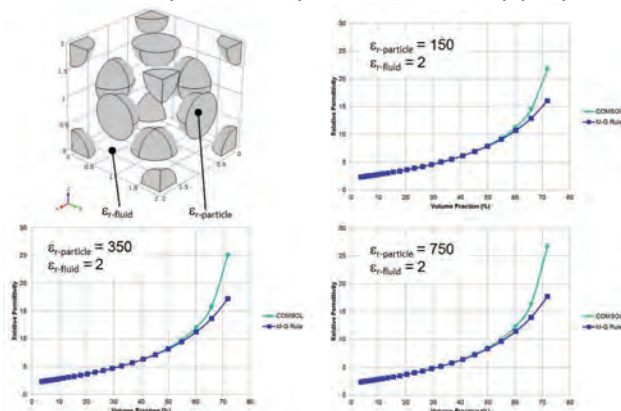


Fig. 13 Quasi-static finite-element simulations of representative volume element (RVE) for body-centered cubic (BCC) periodic cell showing deviation from mixing formula.

Deviations between numerical simulations and mixing formulas can be seen in the results included for the quasi-static RVE simulation of FCC unit cell, and are a common artifact of these and simulations of other particle configurations. This has also been observed experimentally, and the basic behavior is a function of both particle and background permittivity, and the interfacial charge, or double layer that

exists at the surface of the particle. This becomes pronounced at volume fractions above 50% for nearly all simulations (examined so far) with particle permittivities that are two orders of magnitude greater than the background medium. Statistical trends are being generated for this, and one of the current approaches in the realm of RVE simulations used to capture this behavior is to model it as a lossy charge shell (or capacitance); Fig. 14 shows the RVE topology for BCC and FCC topologies. These are currently being simulated at 3 GHz to capture the lossy behavior of the conductive outer shell (which is modeled currently as an ionic solution close to salt water).

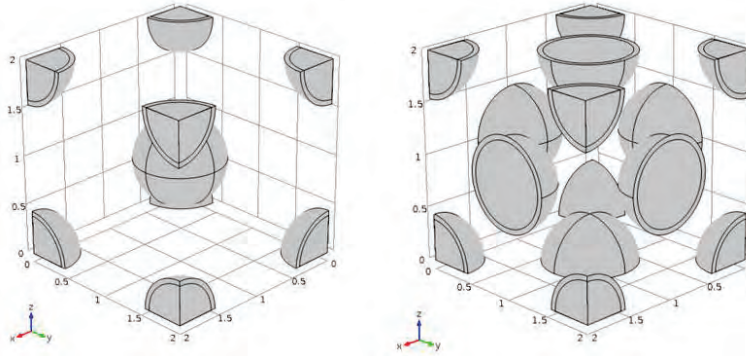


Fig. 14 Core-shell simulations being investigated to develop baseline models of the capacitive double layer in BCC and FCC configurations; quasi-random random configurations are also considered.

An alternative model for calculation of effective complex permittivity at high frequencies has also been explored in this project to more accurately capture the physics of the problem. Fig. 15 provides a notional overview of this proposed approach, which considers the electric double layer as a deformable shell which surrounds the particle. When the external field is applied the charge shell distorts, and when the proximity of particles becomes close (as is the case at high volume fractions) the interaction between particles are modeled as a secondary prolate spheroidal particle defined by the overlapping charge shells. This is given a polarizability that contributes to the overall permittivity in a process which is intended to capture (on first order) the cumulative effect of nearby particles, which can be expanded to a multi-pole multi-body calculation. This approach relies on the large body of work surrounding the calculation of these properties based on known physical phenomena at both the interface between the particle and the background medium as well as the multi-body interaction that occurs when the particle is in the presence of closely-spaced neighboring particles, but it is novel in the capture of these properties as an equivalent source/particle through the perturbation of the local field and the ability to capture this analytically in existing mixing formula.

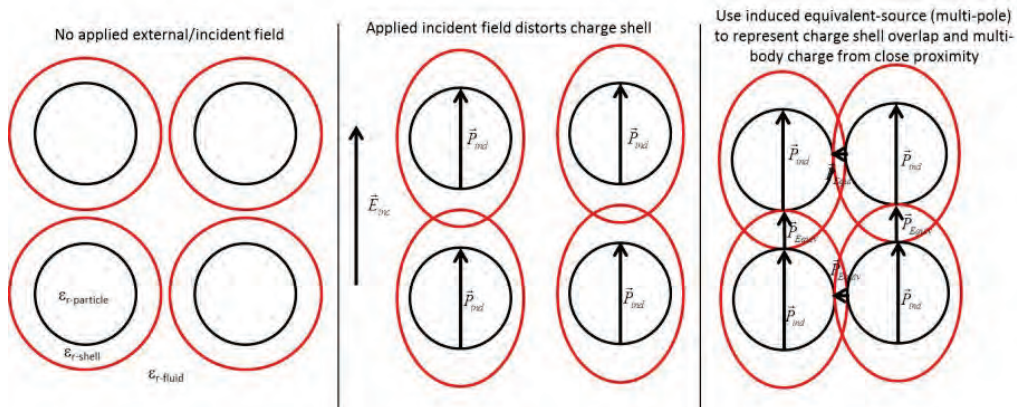


Fig. 15 Core-shell simulations being investigated to develop baseline models of the capacitive double layer and provide a foundation for a multi-pole expansion to capture the multi-body interactions of closely-spaced particles.

2. Control and Mediation of Nanoparticles

- **Goal:** The goals of this objective are to integrate the electromagnetically-mediated control of nanoparticles into electrode topologies that are native to high frequency design and develop locally-controlled anisotropy in electronically tunable composites
- **Expected outcome:** The expected outcomes of this objective are reconfiguration mechanisms with functionality derived from dynamic particle interactions and substrate composites which can provide advanced control of high frequency wave impedance and propagation velocity

i. Facilitate electronic control of particle composition and concentration in RF devices

This project has also developed direct particle scale measurements and models of anisotropic particle interactions with AC electric fields to control orientation and position in various electrode configurations (Fig. 16). Dipole-dipole & dipole-field interactions determine the multi-scale hierarchical structures that lead to a spatial distribution of effective medium dielectric properties in equivalent circuits within devices. Direct knowledge of the interconnections between particle interactions, dynamics, and microstructure allows for actuation and reconfiguration of different states within fluidic devices and in processing nano-composites. Connections of interactions to material properties has enabled the design of core-shell particles with high dielectric constant ferroelectric cores with silica shells and fluorinated surfactants to meet multi-scale design constraints for particle stability, AC field mediated actuation, and device operation.

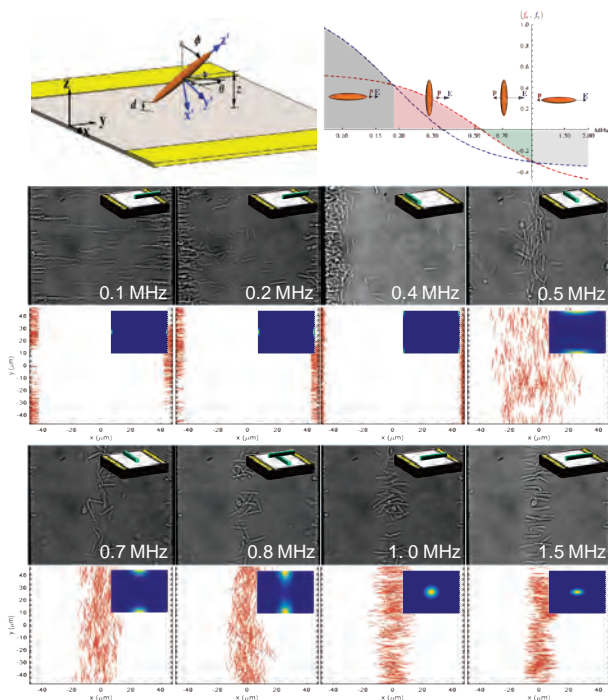


Fig. 16 (right) (top, left) Schematic of rod shaped particles in non-uniform electric field between parallel electrodes.

Variable are defined for theoretical interaction potentials in Monte Carlo simulations. (top, right) Spectrum of dipole potential magnitude along major and minor axes of rod particles that determine their orientation and position in non-uniform electric fields. (bottom panels) Video microscopy images (1st & 3rd rows) and Monte Carlo simulation results (2nd & 4th rows) showing positions and orientations of colloidal rods in inhomogeneous electric fields between coplanar electrodes based on relative complex permittivities along the long and short axes. Insets in experimental images schematically show single rod orientation and position. Insets in simulation renderings show probability distribution in X , Θ , which also shows potential energy landscape via a Boltzmann relationship.

The inset text in the images is the electrical field frequency in MHz; the applied voltage is 3V in all cases.

This project has also been developing additional control authority over particle concentration, configuration, orientation, and position in quadrupolar electrodes by spatially sculpting the electric field amplitude and frequency to lead to non-trivial time averaged particle-field interactions (see Fig. 17). In this work, these control schemes are being combined with the anisotropic particle interactions in Fig. 16 to create hierarchically assembled structures to tune emergent composite material properties within fluidic devices and polymerizable media. The various control modes include: Mode 1: High frequency compression of particles. Changing the amplitude of one pair of electrodes can push clusters of particles to different potential minima depending on field strengths used. Mode 2: Low frequency fields direct particles to electric field maxima, which places them towards electrode edges. Mode 3: One electrode is turned off, which is opposite to the live electrode. It is essentially coupled as a ground electrode. High frequency fields push particles away from the high fields and would eventually get pushed between ground electrodes. This is a transient state. Mode 4: Particles are directed to the highest fields, which is the live electrode. Mode 5a: Different combinations of electrode configurations with different frequencies and voltages can make a wide array of different configurations. This one configuration pushes all particles to the edges. Mode5b: When live electrodes are adjacent to each another, there is a diagonal potential between electrodes, not a circular one in the middle. Cycling the field on and off, or cycling between frequencies also can create different effective minima.

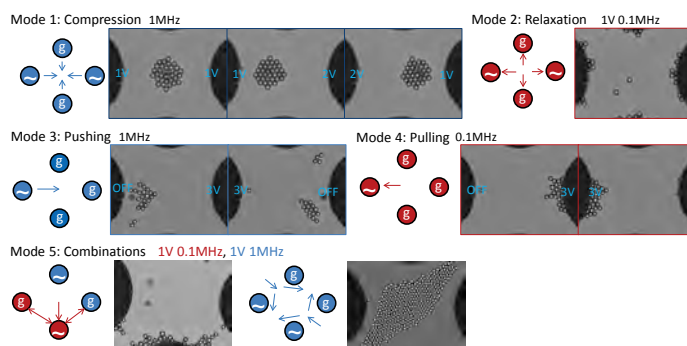


Fig. 17 Controlling spherical particle concentration, configuration, orientation, and position in quadrupolar electrode by tuning amplitude and frequency of dipolar pairs. Results from (left to right, top to bottom) show different actuation modes including compression, relaxation, pushing, pulling, and combinations of modes. In each case, blue indicates frequencies where particles are less polarizable than the medium (and localize at electric field minima), and red indicates frequencies where particles are more polarizable than the medium (and localize at electric field maxima).

We have recently demonstrated quantitative agreement between measurements and models of the system size dependent assembly of quasi-two dimensional (2D) colloidal crystals within interfacial quadrupole electrodes (Fig. 18). Perturbation theory (PT) and Monte Carlo (MC) simulations were used to make thermodynamic predictions of the voltages required to obtain all particles within a crystalline phase for different system sizes. These results show good agreement with video microscopy (VM) measurements of colloidal crystals containing 75-300 particles. Colloidal assembly kinetic trajectories for the same system sizes were quantified from VM experiments using order parameters (reaction coordinates) to capture real-space local and global hexagonal ordering. These trajectories were fit with a Smoluchowski model to extract configuration dependent free energy and diffusivity landscapes (FEL and DL) that capture the microscopic details of particles assembly dynamics. Specifically, landscape features, such as barrier heights and number and local gradients, capture the formation, diffusion, and migration of grain boundaries in polycrystalline states, which are increasingly prevalent for $n > 200$ but vanish to immediately produce single crystals for $n < 150$. These results demonstrate the importance of system size

effects to the formation and annealing of polycrystalline states in colloidal crystallization processes. Ultimately, these results provide a basis to understand how particle-field interactions control the microstructures of spherical particles form in electric fields, which provides a basis for ongoing work to tune the microstructures of anisotropic colloids in fluids and polymerizable media.

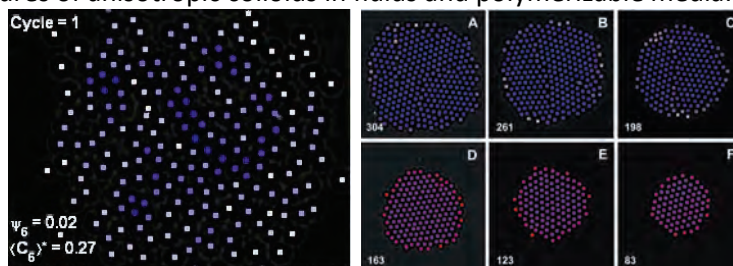


Fig. 18 Controlled assembly of different sized colloidal crystal within a microfluidic quadrupole device shows how defects form that control the ultimate electromagnetic properties of such configurations.

After understanding how different structures form in equilibrium processes, in a subsequent step, we investigated the dynamics of stochastic grain boundary formation and motion, which limits the ability to control and anneal polycrystallinity in colloidal based materials (Fig. 19). In particular, we studied the grain boundary dynamics in quasi-2D colloidal bicrystals formed within inhomogeneous AC electric fields, where voltage acts a surrogate for pressure on induced dipoles. We introduced “low-dimensional” models using reaction coordinates for condensation and global order that capture first passage times between critical configurations at each applied voltage. The resulting model reveals that equal sized domains at a maximum misorientation angle show relaxation dominated by friction limited grain boundary diffusion; and in contrast, asymmetrically sized domains with less misorientation display much faster grain boundary migration due to significant thermodynamic driving forces. By quantifying such dynamics vs. compression, kinetic bottlenecks associated with slow grain boundary relaxation are understood, which can be used to guide the temporal assembly of defect-free single domain colloidal crystals.

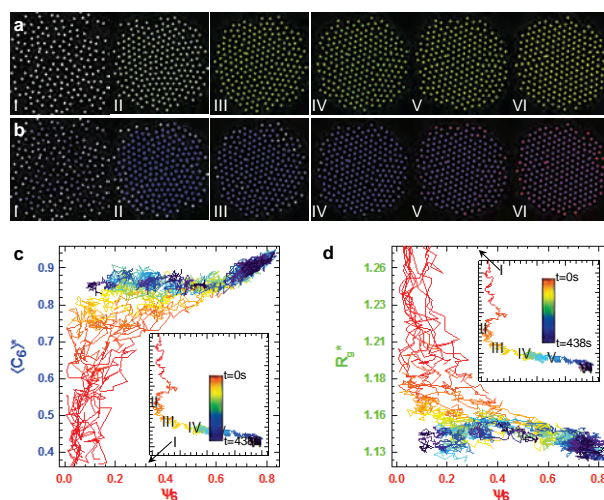


Fig. 19 “Two dimensional” trajectories (*i.e.*, two reaction coordinates) capture coalescence of local domains during fast condensation processes to produce bicrystals that relax to single crystals via grain boundary motion over a broad range of timescales. Microscopy images with particle centers colored using RGB mixing rules for colors represented by two reaction coordinates including (a) ψ_6 and C_6 and (b) ψ_6 and R_g to visualize how global order emerges from local order and during condensation. Ten trajectories following quenches with time represented by an 8-bit linear spectrum (inset scale bar) for (c) $(\psi_6, \langle C_6 \rangle)$ and (d) (ψ_6, R_g) reaction coordinate pairs with inset plots of single trajectories.

Rod shaped colloidal particles have also been prepared for use in the experiments described above to assemble different microstructures in both fluids and polymerized solid composites. In particular, a dispersion of colloidal rods can form various configurations with rod alignment parallel and perpendicular to fields with microstructures including chain and liquid crystal configurations. A demonstration of this reconfigurability using colloidal rods has been performed in several microfluidic-microelectronic devices. Both conductive/magnetic nickel rods and dielectric silica rods have been prepared for this. The silica rods were prepared using a literature method for making silica spheres where a structure directing polymer (PVP) is added. Nickel rods were synthesized using electrochemical deposition. A mixture of nickel sulfate, nickel chloride and boric acid was combined to form the nickel plating solution. To create uniform rods, a porous anodic alumina (PAA) film or very uniform 200 nm diameter pores was coated with a film of copper about 300 nm thick. A platinum counter electrode was connected to the power supply with current density of 10m A/cm², which allowed for an electrochemical reaction where the nickel sulfate was reduced to form nickel metal in the pores, creating uniform rods.

Initial characterization of both rods has included measurements of their interactions in the absence of fields as well as DC and AC fields at different field amplitudes (Fig. 20). Video microscopy of particle trajectories in the absence of fields is used to characterize their Brownian translation and rotation, which is important to understand their directed motion in fields. These measurements also reveal how electrostatic, van der Waals, and gravitational forces control the interaction of the particles with the substrate in different media. Measurements of electrophoresis in DC fields are used to characterize the particle surface charge and medium conductivity. This information is used in conjunction with frequency dependent dipolar interactions in AC fields to obtain complete characterization of the particle and medium dielectric spectra and their connections to particle assembly and dynamics in electric fields. We are currently using this information to assemble rod shaped particles in microfluidic devices and prepolymer media using parallel and quadrupolar electrode configurations (Fig. 20).

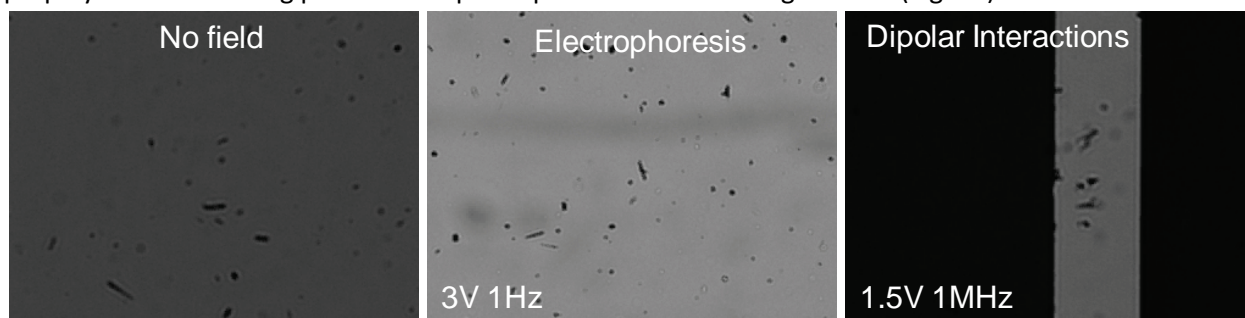


Fig. 20 Video microscopy measurements of: (left) rod shaped particle Brownian translation and rotation and substrate interactions in the absence of a field, (middle) rod shaped particle electrophoresis and charge properties in DC electric fields, and (right) particle dielectric spectra and interactions vs. AC field frequency. This provides complete characterization of particle properties and interactions for assembly of microstructures in fluid and prepolymer media.

This project has also demonstrated feedback control over the local concentration, configuration, and dimensionality of spherical colloids in aqueous and non-aqueous media. For example, Fig. 21 shows how negative and positive dielectrophoretic forces in high frequency AC electric fields in a quadrupolar electrode configuration can be used to manipulate particles between dilute, disordered fluid configurations and concentrated, hexagonal close packed states. This is done in real time using image analysis to track particle centers and compute order parameters to characterize the current state, which is then used to tune the field amplitude and frequency in a function generator (based on control laws measured in Fig. 21). In another example in Fig. 22, electrophoresis, electroosmosis, and

dielectrophoresis are used in integrated micro- electronic/fluidic device to control the number of particles and concentration. Combining this approach with the one in Fig. 21 allows control over particle number, concentration, and configuration, which can be used to control composite dielectric spectrum. A final additional level of control authority is demonstrated in Fig. 23 where compression of two dimensional configurations under negative dielectrophoretic forces buckles particles into three dimensional architectures within the quadrupole. All of these methods are currently being adapted to anisotropic particles, which have additional orientational degrees of freedom relative to the field for dilute single particles and relative to each other in concentrated configurations (where various isotropic and liquid crystalline phases are obtained, i.e. nematic, smectic).

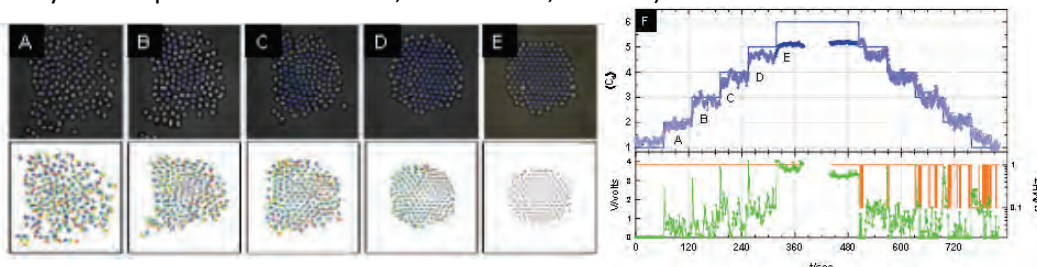


Fig. 21 Controlled assembly and disassembly of colloidal crystal within microfluidic quadrupole device.

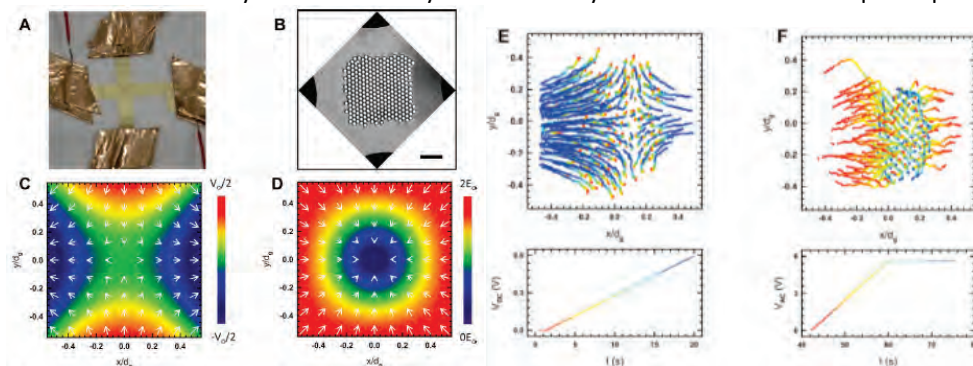


Fig. 22 Quadrupole design at macro and micro scales, flow and electric fields, particle and voltage traces.

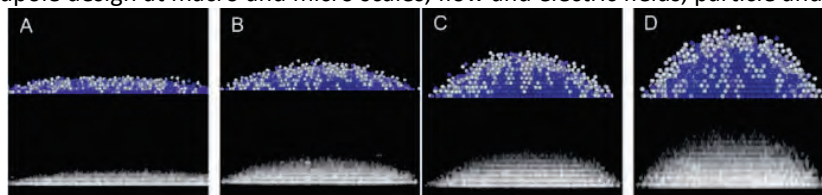


Fig. 23 Simulated and experimental cross sections of reconfigurable 3D periodic crystalline configurations assembled in high frequency fields in quadrupole electrode in non-aqueous dimethylformamide media.

ii. Determine maximum flow rates and effective viscosity within capillary architecture

Direct measurements of particle dynamics vs. particle concentration and configuration in experimental has been used to obtain microscopic estimates of dispersions viscosities for comparison with macroscopic measurements and microfluidic flow studies in numerical simulations similar to the RVE simulations. In particular, measurements of particle time-scale dependent diffusion via mean squared displacements of particle centers will be related to time-scale dependent viscosities via well-established theories. For anisotropic particles, these diffusion coefficients and viscosities will have directional components based on particle orientations in electric fields or flow fields.

iii. Use particle alignment to create tapered and ferroelectric anisotropy in antenna substrates

A co-planar waveguide (CPW) bandpass filter has been examined in this project as a candidate device topology for the integration of anisotropic and/or ferroelectric materials. Fig. 24 shows the metallization (left side) and field distribution (right side) for the nominal CPW topology at 20 GHz. The structure is a very common transmission line topology for microwave and millimeter-wave applications since it provides mode-free transverse electromagnetic wave propagation over a very large bandwidth (from DC to 10's or 100's of GHz depending on the dimensions). It also provides several advantages for this component of project. Of most significance, it has a three electrode topology that can be utilized to provide anisotropy in a nanocomposite in a direction which will have the highest electromagnetic visibility to the propagating waves. In this regard, the signal line can be excited with low-frequency (< 10 MHz) for electric-field assisted mediation of particles that are placed over the two longitudinal slots that separate the signal line from the grounds. This project has supporting work that is examining the alignment of particles across similar electrode structures.

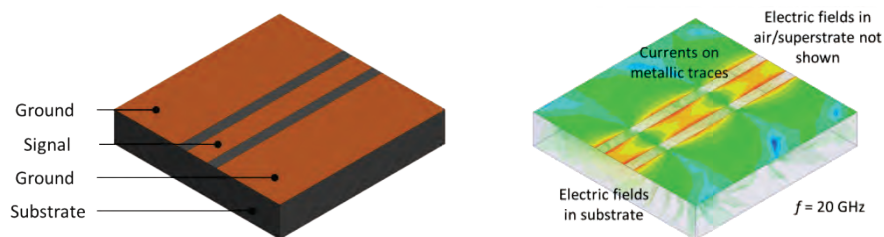


Fig. 24 (left) A co-planar waveguide (CPW) transmission line and (right) its simulated response at 20 GHz..

A band-pass filter topology has been created from this transmission line topology by perturbing the signal line with an H-shaped resonant slot (Fig. 25). The notional graph of the band-stop filter response that is being engineered into the device topology is shown next to the filter; scattering (S)-parameters are used for this, which in this context represent the magnitude of the ratio of incident power to the power transmitted through the device (much like the transfer function of a system). This has been examined to create a demonstration vehicle which is very sensitive to changes in any substrate and/or superstrate materials. A design frequency of 20 GHz has been chosen to provide a small physical dimension of the RF device so material coupons can be generated rapidly for testing.

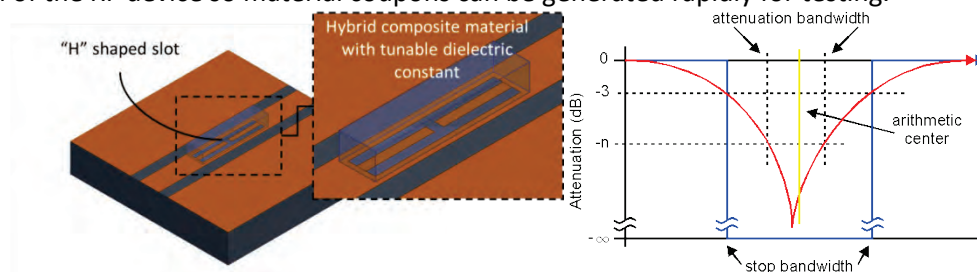


Fig. 25 (left) CPW H-slot (stop-band) filter and (right) notional filter response using scattering (S)-parameters.

Fig. 26 shows the simulated response of the filter topology in which a very small rectangular-shaped composite material has been patterned over the H-slot (Fig. 25). This shows the response of this as the dielectric constant of the material is swept over the range $1 \leq \epsilon_r \leq 50$, and can be used to emulate the use of a fluidic mechanism that can alter the orientation of rod-shaped particles to increase the anisotropy in the fluid or show the response of a ferroelectric material changing from an applied DC bias. This level of tuning without the development of second-order resonances or other higher-order effects is unique to this device typology.

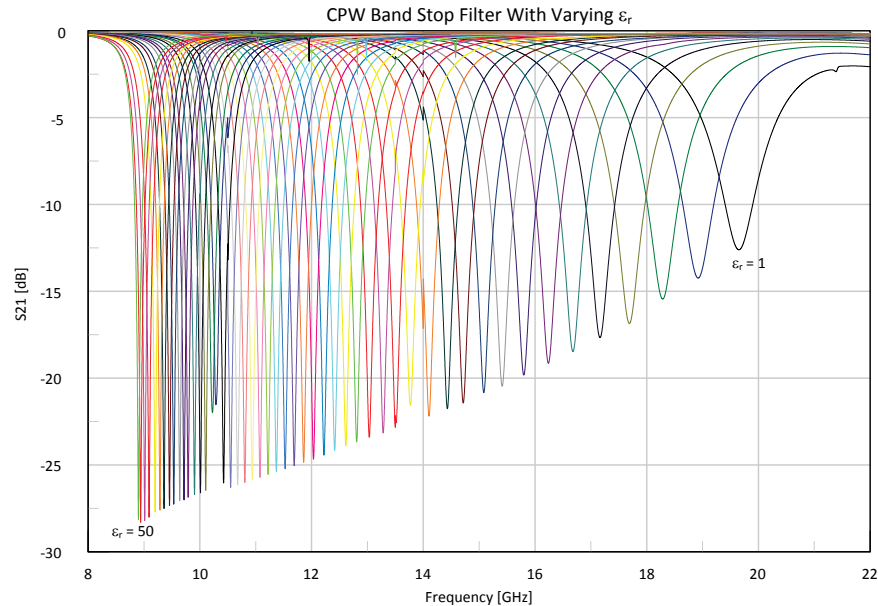


Fig. 26 Simulated performance of the CPW H-slot (stop-band) filter when varying the dielectric constant of the patterned nanocomposite from $1 \leq \epsilon_r \leq 50$.

Several methods were also examined to develop high performance substrates for antenna using the alignment of high aspect ratio BT in a polymer-ceramic nanocomposites-matrix. The inclusion properties are clearly important in this regard, and are a key component of this project, but the trade-offs between loss and loss mechanisms associated with the background matrix material and the dispersal of these inclusions into the matrix are being examined for a range of flexible materials that will be suitable for high frequency antenna design and tuning. Polydimethylsiloxane (PDMS) polymer is one of the current materials that can be mixed with the ceramic powder and fabricated to make it a soft and flexible solid composite substrate, and it can be used to provide proof-of-concept demonstrations, but it is a lossy material that is not well suited for high frequency applications. Moving away from this well-known background medium has provided several opportunities to examine other avenues for dispersal into the medium, and one major ongoing effort in this process for improving the dispersion stability of nanoparticles and increasing the properties of polymer nanocomposites is modifying the surfaces of nanoparticles.

3. Design and Operation of Reconfigurable Antenna Systems

- **Goal:** The goals of this objective are to integrate nanoparticle-driven reconfigurable and tuning into the design space of high frequency electromagnetic devices and integrate the thermal behavior into the electromagnetic operations related to sensing and communication
- **Expected outcome:** The expected outcome of this objective will be the design of advanced reconfigurable antennas and tunable circuits with multi-physics models that incorporate the thermal properties of nanoparticle-based material systems in their analysis

i. Examine reconfiguration mechanisms based on EM mediated particle assembly and fluid flow

The first antenna reconfiguration mechanism under investigation is a broadside gap (or edge-coupled electrode) with a tunable dielectric material (or tunable 'brick') placed above the host substrate and the metallization of the antenna. This is the most common electrode configuration and it offers many opportunities to exploit the dynamic changes in permittivity and/or conductivity from fluidic,

ferroelectric, and/or electrokinetic mechanisms; it is also used in the EM mediated particle control experiments in this work (along with other multi-pole electrode configurations). The three gap topologies shown in Fig. 27 (straight, circular, and triangular) are included here to illustrate the basic topology and to demonstrate the impact of their topology as a reconfiguration mechanism of the slotline-fed loop/dipole antennas shown in Fig. 28 – the tunable material in this case resides on the location identified as the ‘location of the gap electrode’.

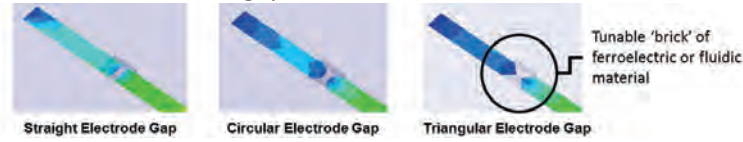


Fig. 27 Electrode gap topologies used in the simulation of the reconfigurable antenna to study the sensitivity of the design to the electrode gap; this has a pronounced effect in EM mediated control of particles when control is desired across this gap.

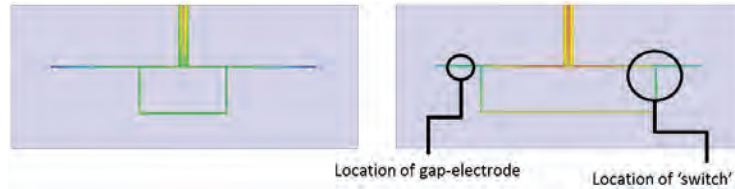


Fig. 28 Simulated surface current on two variations of a pattern and frequency reconfigurable coplanar slot-fed dipole/loop antenna showing the location of reconfiguration mechanisms.

In this configuration, the gap acts as a capacitive load that creates an effective lengthening of the antenna as the dielectric permittivity of the material in the ‘brick’ increases. This is discussed more in the next section on antenna design, but the ‘brick’ in this context can be used represent a variety of fluidic and EM-mediated mechanisms at high frequencies and ties into the effective medium property work also being performed in this project. From a reconfiguration standpoint, it has been demonstrated in both current and prior work that the gap/electrode topology plays a significant role in the low frequency behavior (through the structuring and inhomogeneity of the applied field). However, at high frequencies the gap plays a more generalized role in the system-level operation of the antenna and/or circuit (in the frequency ranges considered in this project). This can be seen by observing the real and imaginary impedances in Fig. 29; the 1.0 GHz to 4.5 GHz frequency range includes the first resonance of the reconfigurable antenna shown on the right side of Fig. 27 (nominally 3 GHz).

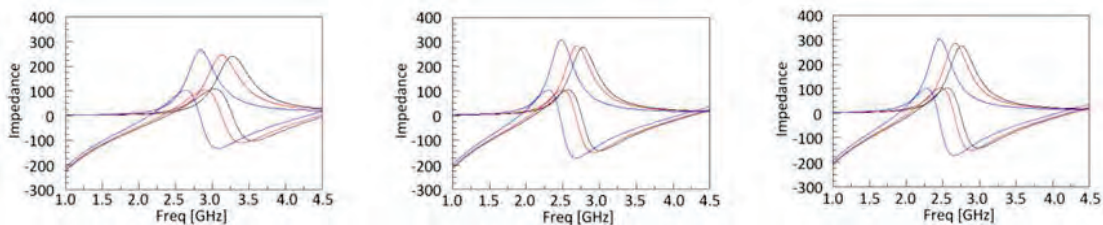


Fig. 29 Simulated impedances of the antenna in previous figure using air [black], randomly aligned BSTO nanorods in oil [red] and aligned BSTO nanorods in oil [blue] for the dielectric material loading the gaps.

The three cases shown in Fig. 29 provide one key observation. Namely, that that each of these topologies remains generally similar in the response as the permittivity of the ‘brick’ is changed from using air ($\epsilon_r = 1$) [black], randomly aligned BSTO nanorods in oil ($\epsilon_r = 10$) [red], and aligned BSTO nanorods in oil ($\epsilon_r = 100$) [blue]. For antennas and circuits with smaller feature sizes this will obviously play a more pronounced role, and there are certainly other topologies that can influence this in a more substantive way, but for lower-frequency devices (e.g., from 10 MHz up to 10 GHz) these gaps can be tailored more for the desired EM-mediated response and used to facilitate particle-level control. This

illuminates some interesting new dimensions to the design space for the development reconfigurable antenna and tunable circuits that have been uncovered in this work.

A number of other antenna topologies have been investigated in this project that can be enabled by the EM mediated particle assemble and fluid flow. Fig. 30 shows the CAD model of the CPW folded-slot antenna that has been designed to work at 20 GHz. This is the modified version of this antenna which features that same H-slot topology with a patterned section of nano-composite material. This antenna has a similar field structure as the transmission line but is a standing wave device. This implies that the behavior may not be directly transferrable, in that the same tuning range of the filter may not be achievable, but the investigations of the antenna topology have demonstrated that a large degree of tuning is possible.

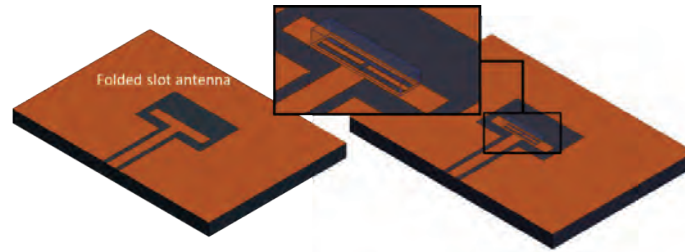


Fig. 30 (left) Folded slot antenna and (right) modified design that is integrated with an H-slot (stop-band) filter patterned nanocomposite.

Other efforts (based on a previous AFOSR-funded project) have also been pursued in this project to examine the use of anisotropic effective medium properties in fluidic dispersions and/or ferroelectric nanocomposites in reconfigurable antenna design. Fig. 31 shows the polarization-reconfigurable crossed microstrip patch antenna (on the left) and its equivalent circuit model (on the right). This antenna was originally engineered to provide polarization switching by displacing a fluid with a high dielectric constant (shown in red) over the gap to capacitively load and activate sections of the antenna. This new design has been re-engineered to include the ability to utilize the effective medium properties of the fluid or composite to provide frequency tuning in the polarization reconfigurable states.

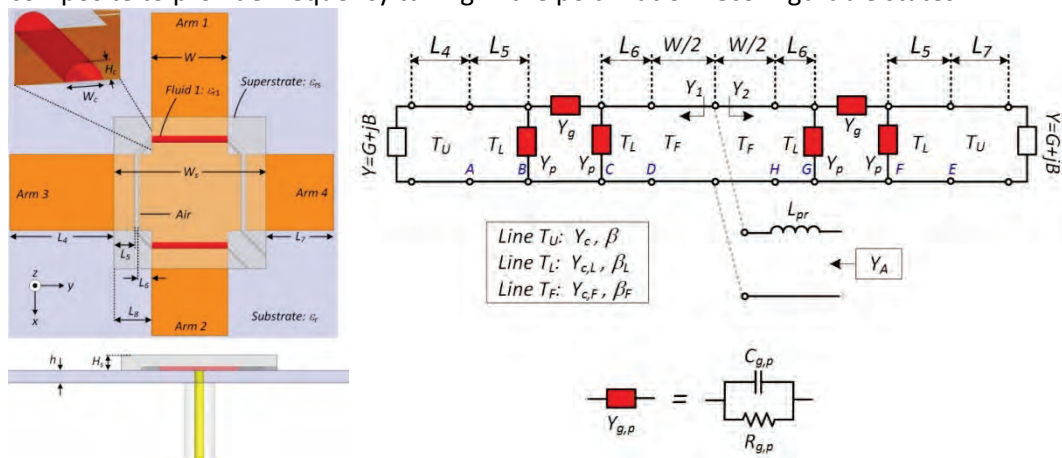


Fig. 31 (left) Polarization-reconfigurable crossed microstrip patch (right) and its equivalent circuit model with tunable fluidic and/or nanocomposite materials shown in red.

A multi-scale equivalent circuit model of the antenna in Fig. 31 has also been reformulated to study the fundamental connections between the multifunctional materials and the design of the antenna. This now includes this ability to tune the frequency of the antenna by altering the dielectric constant of the

fluid and/or nanocomposite. A comparison of full-wave finite element simulations and the multi-scale circuit model calculations has been included in Fig. 32. This study shows the tunability of the antenna when sweeping the dielectric constant of the material loading the capacitive gap in the polarization reconfigurable antenna from $10 \leq \epsilon_r \leq 80$ using lossless materials and materials with a dielectric loss tangent ($\tan \delta$) of 0.02. These results demonstrate that the impact of material properties can be accurately captured and used to study the connection between antenna metrics (in particular its radiation efficiency). This antenna has also been re-engineered to feature conductive fluidic materials (liquid metal alloys).

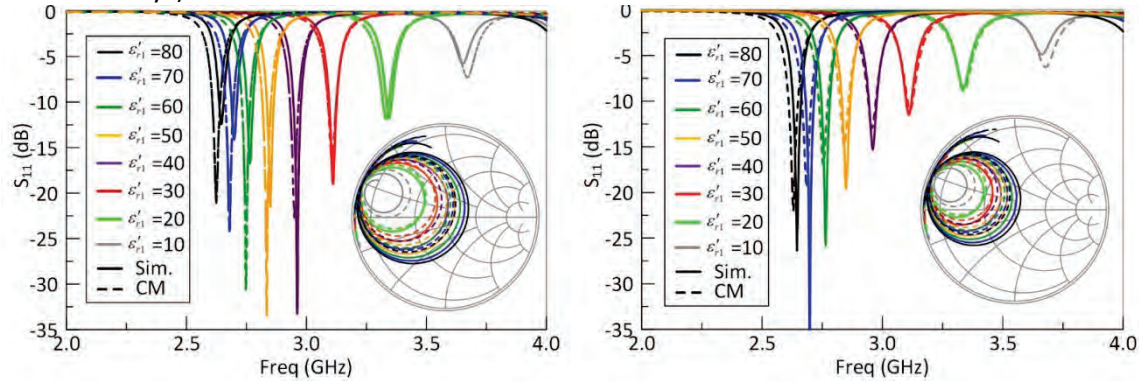


Fig. 32 Comparison of finite element simulations (Sim.) and the multi-scale circuit model (CM) while sweeping the dielectric constant of the material loading the capacitive gap in the polarization reconfigurable antenna from $10 \leq \epsilon_r \leq 80$; (left) lossless materials and (right) materials with a dielectric loss tangent ($\tan \delta$) of 0.02.

A liquid metal reconfiguration mechanism was also designed and fabricated in this project as a switching mechanism for a frequency-reconfigurable edge-fed microstrip patch antenna. The antenna was designed to operate in either the 2.4 GHz Industrial Scientific Medical (ISM) band or the 1.6 GHz L2 Global Positioning System (GPS) band and a partitioned fluidic manifold was bonded to the top of the antenna to enable the pressure-driven displacement of a low-loss dielectric fluid and the liquid metal from a reservoir atop the patch to switch between the two antenna states. In a broader context, this illustrates the use of fluidics as an alternative to RF switches for reconfigurable antennas.

This reconfigurable antenna (Fig. 33) resides on a Duroid 5870 substrate, which is a Teflon and woven E-glass composite with excellent microwave properties. The antenna's metallization (shown in yellow on the left diagram in Fig. 33) was synthesized by overlapping two independent edge-fed microstrip patches with resonant lengths L_1 and L_2 corresponding to the 1.6 GHz GPS and 2.4 GHz ISM bands, respectively; each design had identical widths W . The two patches are aligned at their respective inset feed point using insets s_1 and s_2 (these gaps provide the RF impedance match for maximum power transfer from the narrow microstrip line and facilitate high radiation efficiency) and lateral slots of width g were removed from the larger patch in the overlaid configuration to electrically isolate the two designs. In this setup, the antenna reconfigures by simultaneously altering the electrical continuity across the three gaps – hence, the liquid metal acts a continuous switch across the two gaps. The three-piece fluidic manifold in the middle of Fig. 33 was fabricated from polydimethylsiloxane (PDMS) using a reverse mold fabricated by a low cost 3D printing machine. It was plasma-bonded to the antenna and a laser machining tool removed the spin-coated PDMS layer from beneath the PDMS fluidic channels.

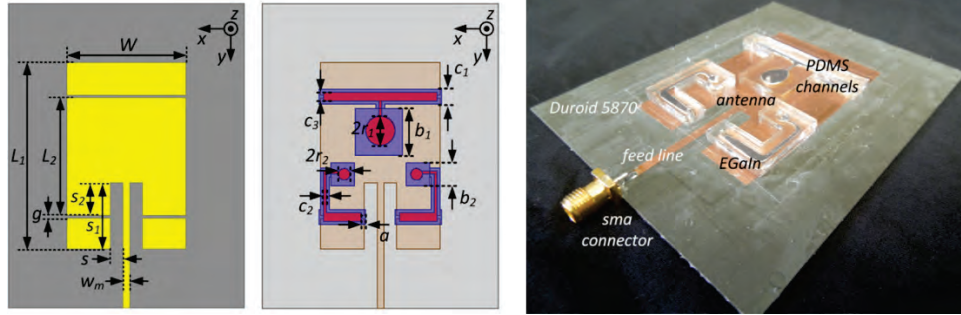


Fig. 33 Top-down view of the antenna with metallization shown in yellow (left), fluidic manifold atop of the antenna; red indicates the fluidic channel network and purple indicates the overall footprint of the fluidic manifold (middle), and fabricated antenna (right).

Hydrocal 2400 (electronic liquid) and EGaIn (liquid metal) are the two immiscible fluids used in this reconfigurable antenna. The Hydrocal 2400 provides an insulating low-dielectric and low-loss material that will not oxidize the EGaIn and it is also viscous enough to push the EGaIn without forming droplets; prior to loading the channels with these materials, a mixture of 5% polytetrafluoroethylene (PTFE) was flowed through the channels and air-dried to coats the inner surface of the channels and reduce oxidation, improve wetting, and to prevent EGaIn from leaving a residue on the walls. The diagrams in the middle of Fig. 33 show both states of the antenna. In State 1, the viscous dielectric liquid (red) fills the slots while the liquid metal (blue) resides in the circular reservoirs near the center of the patch so there is no electrical continuity across the gaps. To push the liquid metal in and out of the channels, and to avoid oxidation of the EGaIn, the viscous liquid has to be on either side of the liquid metal as it flows from the reservoirs. In State 2, liquid metal flows across the slots and effectively elongates the antenna by connecting the inner and outer sections - this operation makes its matched impedance bandwidth (where it can radiate efficiently) operate at a lower frequency. Fig. 34 shows the measured and simulated voltage standing wave ratio (VSWR) and co-polarized radiation patterns in the E-plane and H-plane. Measurements of the antenna (in version 1) showed an impedance mismatch for State 2 (not observed in simulation), which arose as a result of the fabrication process. A second antenna (version 2) was designed by decreasing the inset s_1 (keeping s_2 the same) in order to correct for the impedance mismatch.

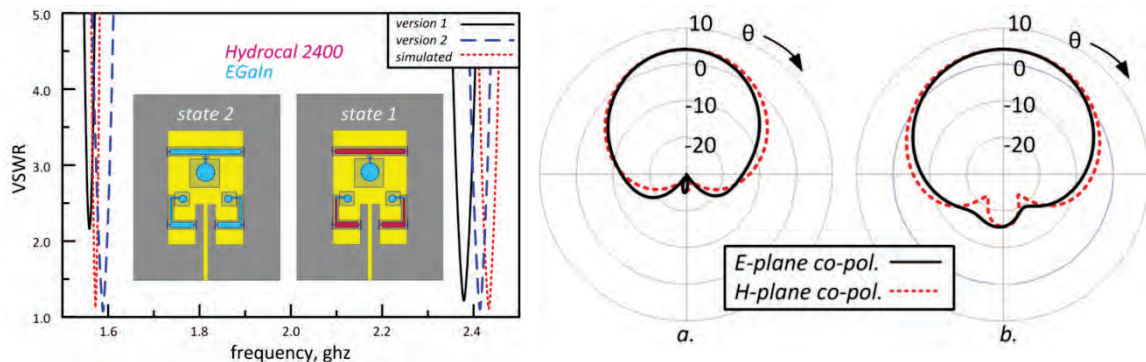


Fig. 34 The VSWR of the antenna operating in its two states (left) and Fig. 4 Simulated radiation patterns of the antenna. The units of the graph are in dB. The antenna's cross polarizations fall outside the dynamic range of the plots.

ii. Engineer frequency and pattern reconfigurable antennas and dynamic circuits

The reconfigurable antenna shown in the top of Fig. 35 is a canonical version of the simulated antenna shown in Fig. 28, and the green and blue lines have been overlaid to provide a basic physical explanation

of the design. A number of other variations of this have been examined in this project to explore the use and operation of fluidic reconfiguration mechanisms. The conceptual operation can be explained by examining the overlaid diagram and the three primary configurations below (the loop, the split loop, and the dipole). Each of these three variants represents a means to achieve a fundamentally different radiation pattern. Pattern shaping (directionality) can be achieved through reconfiguring the split loop, and polarization can be achieved by reconfiguring between the loop and dipole. These three configurations can be achieved by altering the two electrokinetic switches, and all variations can be reconfigured in frequency through the tunable capacitors (shown as pressure-driven mechanisms). This design and several other structures including reconfigurable filters have been used to provide the correct impedance match and desired performance metrics.

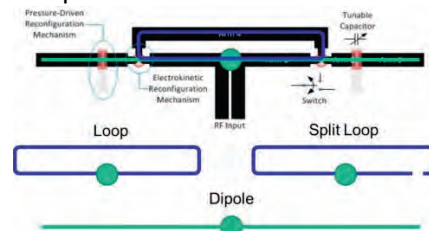


Fig. 35 Notional model of the reconfigurable antenna shown in Fig. 3.2 to illustrate the three basic reconfig.d states of the antenna.

A polarization-reconfigurable substrate-integrated waveguide (SIW) cavity-resonator slot antenna has also been engineered in this project. The CAD model of the revised design has been included in Fig. 36. This new design has taken the large linear channel (that simple covered the entire slot) and transformed it into a serpentine channel that makes multiple contacts with the slot to short out the correct component of the slot and provide reconfiguration that is identical to the previous design. This design also features the added benefit that the frequency of the antenna can also be tuned in discrete steps based on the number of sections of the serpentine channel that are activated. This has enabled the automation and control.

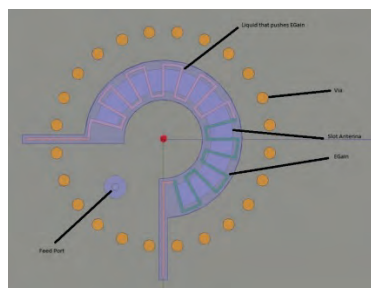


Fig. 36 Polarization-reconfigurable substrate-integrated waveguide (SIW) cavity-resonator slot antenna with a serpentine channel that flows liquid metal in the microfluidic channel to enable reconfiguration.

A fluidic control system for the antenna in Fig. 36 was examined in this project to examine the pragmatic use of fluidic systems in RF/microwave applications. The antenna in Fig. 37 is similar to the antenna in Fig. 36; it is based on a circular cavity resonator with a circular resonant slot that is etched into one side of the cavity. The cavity is created using a circular via fence and the design is synthesized on an FR-4/G-10 substrate. The fiberglass/epoxy composite substrate is not ideal for antenna performance due to its high losses at RM/microwave frequencies but it was chosen so the whole structure could be fabricated using commercial printed circuit board (PCB) techniques and integrated with electronics for control and fluidic sensing. A fluidic manifold is placed atop the structure which contains an EGaIn plug of a specified length which can be displaced across the slot to electrically close one section of the slot and control the

polarization of the antenna while fixing it at a constant frequency. The top-middle diagram in Fig. 37 shows the CAD model of the antenna structure used for full-wave electromagnetic simulation and the bottom-middle diagram shows the electric field distribution at the design frequency of 2.45 GHz when the metallic fluid plug is in the bottom portion of the fluidic channel (the heat-map shows the maximum electric field in the substrate where the slot is, and where the aperture is radiating).

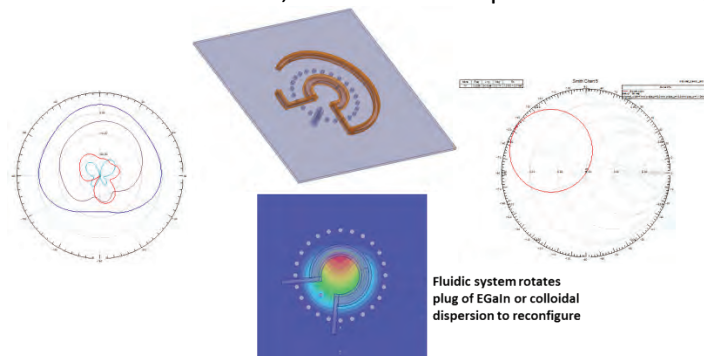


Fig. 37 Simulated radiation pattern (left), CAD model (top-middle) and electric field in one state (middle-bottom), and impedance plotted on a Smith chart from 2 GHz to 4 GHz (right) – the circular curve illustrates that the antenna is resonant and the passing of this curve through the center of this chart demonstrates that the impedance of the antenna is matched to the coaxial line feeding the structure.

The numerically simulated radiation pattern and input impedance are shown in the left and right diagrams in Fig. 37. Cumulatively, this information indicates that the antenna has acceptable polarization purity but a good impedance match so the design was fabricated. Fig. 38 shows several images of the antenna. The left side shows the PLA fluid manifold that was fabricated using low cost 3D printing technology and the H-bridge motor driver IC that powers that bi-directional microfluidic pump shown in the lower-right hand side of the middle image. This middle image also shows the Teensy 2.0++ microcontroller board and additional surface mount devices (SMD) used to fabricate the fluidic sensing and control circuits. This represents a very unique advance with respect to other fluidic antenna reconfiguration technologies; in particular, the two lines running next to the circular cavity contain probes which make contact with the fluids that reside in the fluidic manifold. A small section of a third immiscible fluid with a known resistivity (water) has been added into the channel but isolated from the electromagnetic performance of the antenna – in this configuration the microcontroller reads the position of the EGaIn fluid plug, which is pushed by low-loss dielectric fluids (oils), by monitoring the resistance change created by the water. The antenna can then accurately, and autonomously, change the polarization of the antenna by interacting with the fluidic reconfiguration mechanism.

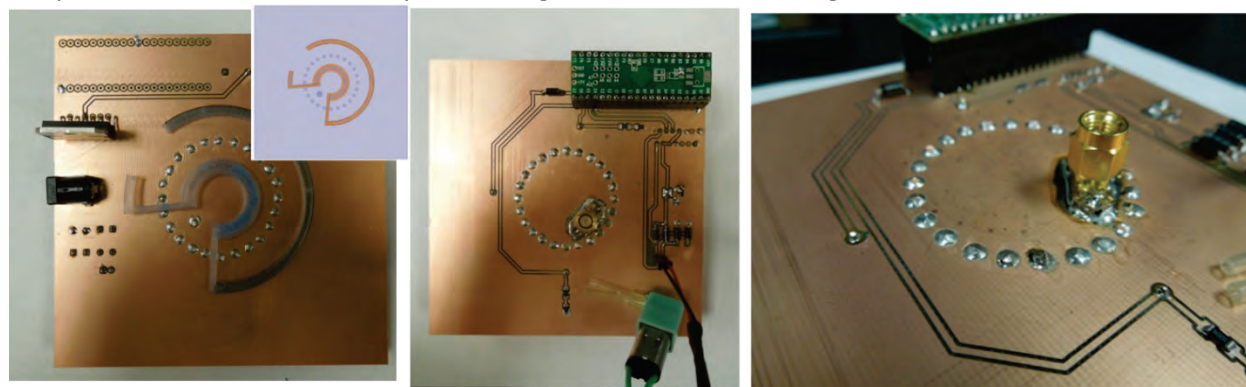


Fig. 38 Images of the polarization reconfigurable antenna system with integrated RF, pumping, sensing, and control electronics.

iii. Encapsulate effective EM and thermal properties of dispersions

A thorough investigation of mixed thermal and electromagnetic properties has been performed in this project for a number of material systems. This included a numerically-derived multi-physics model using COMSOL, and one of the intermediate steps in this process is developing a similar model for the flexible load-bearing substrate of the antenna (chosen as a target application space). Inclusions of high aspect ratio ferroelectric particles and structural reinforcement materials are expected to be present in the matrix, so the co-design of structural and electromagnetic properties has been included into this effort. The material design space for a composite structure is being analyzed from the standpoint of balancing the mechanical and electrical properties, and the initial matrix medium was Rohacell foam. This is not flexible, but it provides a low-loss and low weight-density material that is available for experimental work and other foams, etc. are being considered to provide the deformability for the flexible antenna system. The candidate inclusions shown in Fig. 36 were modeled as fiberglass (for structural reinforcement) and colloidal rutile (for dielectric enhancement). This includes scenarios with closely-spaced particles ('near' spacing in Fig. 36) and fibers as well as some more remotely-spaced inclusions ('far' spacing in Fig. 36).

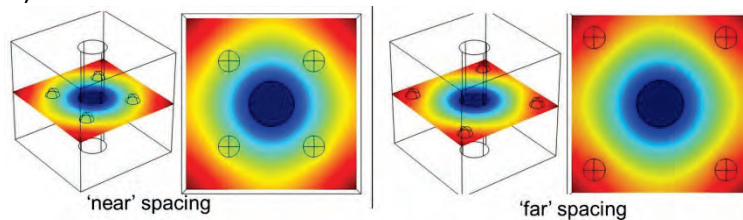


Fig. 39 Two variations of RVE models for structural and electromagnetic co-design of nanocomposites and their constituent materials.

The tensors for tensile strength, compressive strength, and Young's modulus were all studied as a function of volume fraction using the basic rule of mixtures. The anisotropic effective dielectric constant was calculated according to the multiphase Maxwell Garnett mixing rule, and the mixture design space was restricted to volume fractions below 40%. This limit has been determined 'practical' for many of the large scale lab experiments; from past mixing experience, volume fractions up to this point can be easily achieved and past this point and above this the mixing process becomes much more difficult. Furthermore, the higher volume fractions can increase the structural weight to the point where flight in a potential UAV application could be diminished. Using this process, it was found that a wide range of dielectric constants can be achieved over the design space, and that a 20%-20% mixture of rutile and fiberglass inclusions into the foam matrix can increase the structural strength while maintaining a low overall weight.

4. *Evaluation of Superconfigurable Antenna Test-Bed*

- **Goal:** The goals of this objective is to integrate electromagnetic, thermal, and mechanical capabilities into the design and operation of a superconfigurable antenna system
- **Expected outcome:** The expected outcome of this objective will be the demonstration of an automated test-bed for superconfigurable antennas which can provide closed-loop control of frequency-reconfiguration, electromagnetic compensation of physical deformation, and thermal management

i. Integrate reconfigurable antennas into deformable structure

One of the key features of this work is the design of superconfigurable antenna structures. The reconfigurable dipole/loop antenna discussed in the previous sections has also been examined as a candidate for this, but a new design based on a microstrip patch antenna was developed to provide a hybrid antenna-pump ('pumptenna') structure. The diagram on the left side of Fig. 40 shows a notional cross-section of the antenna topology and the basic operation of the device. As of this report, the current goal for this antenna is to integrate a mechanism which can deform a centrally-located reservoir within the antenna that is connected to a capillary structure with single-leaf check valves. This is a very common single-action pumping topology, but it has not been developed as an integrated platform for both pressure-driven fluid displacement and electromagnetic radiation. This consolidated the pumping mechanism into the antenna itself, currently an electroactive polymer (EAP) or piezoelectric material is being considered for this, and the design has uncovered a very unique operational space.

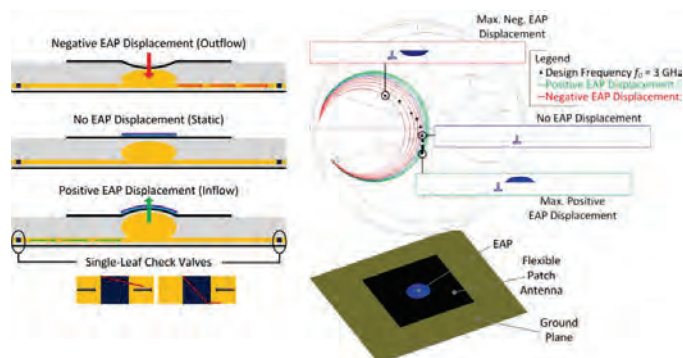


Fig. 40 (left) Basic operation and design concept for the integrated antenna fluid displacement system and (right) Model of a 3 GHz 'pumptenna' and simulated results illustrating the impact of deforming the central region using an electroactive polymer (EAP).

The Smith chart on the upper-right side of Fig. 40 includes simulated results for the structure in the lower-right side of the Fig. 40. These provide several very key pieces of information related to the feasibility of the design and its overall practicality (some can deduced from inspection and color coding). Namely, the red and blue curves on this Fig. illustrate that the structure will operate in a more stable electromagnetic range when the displacement is positive, and become less stable when the displacement is negative. The black dots on each of these curves indicate the 3 GHz design frequency (which is also more stable for positive displacement). There are many possible variations of this design which can provide useful insight into the fundamental behavior of these structures as well as practical information on their integration and performance. A study on the feasibility of this concept using conductive fabric was also performed and a microstrip patch antenna was fabricated (Fig. 41). The antenna was elastic, but the RF properties of the fabric were not conductive enough to use for this work.



Fig. 41 (left) Cross-section of the flexible patch antenna and (middle, left) pictures of a prototype antenna after fabrication using a conductive and elastic fabric.

The 'pumptenna' concept was demonstrated experimentally. Fig. 42 shows the fabricated antenna (left) as well as a comparison of measured and simulated results; the metric for comparison is the voltage standing wave ratio (VSWR). The fluidic components of this antenna were created on a commercial (off-

the-shelf) 3D printer and FC-70 (a heat transfer fluid) was chosen as the base fluid for measurements. The antenna was designed for an operating frequency of 1 GHz to ensure the tolerances of the commercial 3D printer would not impact the performance of the design. This antenna performed as expected and the system is currently being prepared (sealed for leaks, etc.) to be measure in the anechoic chamber for radiation pattern testing.

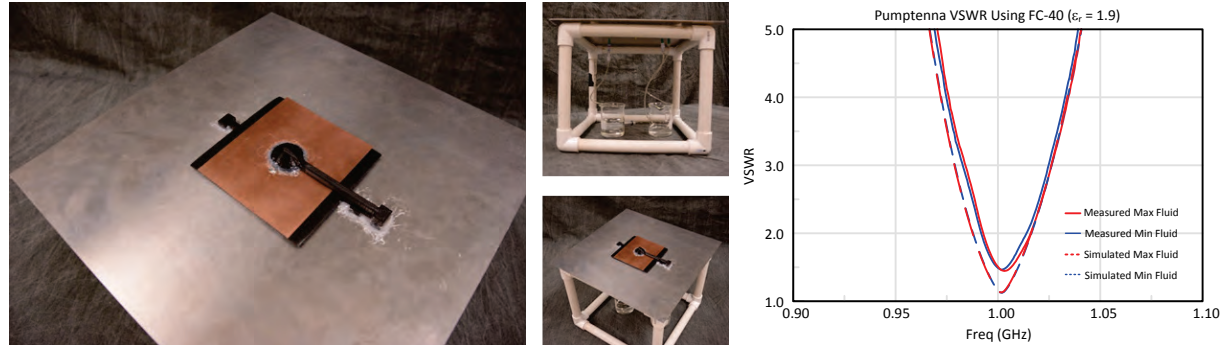


Fig. 42 Fabricated and fully-operational 'pumptenna' using heat-transfer fluid

A series of simulations were also performed to examine the impact of cavity shape on the performance of the design. Fig. 43 shows a subset of the cavity topologies that were examined to study the shape and size of the deformable cavity; this will impact both the flow rate as well as the antenna performance. It was found that the size played the larger role in the performance of the antenna, as was expected, but the shape of the cavity also impacted the performance. These results follow the general trends for a cavity perturbation and mixing formulas were used in the simulation to examine the range of materials (including losses) that could be used in this system. It is instructive to recall that the purpose of this exercise is to examine the ability to functionalize the antenna with fluidics in a way that does not create changes in its performance (an inverse problem as that of reconfiguration).

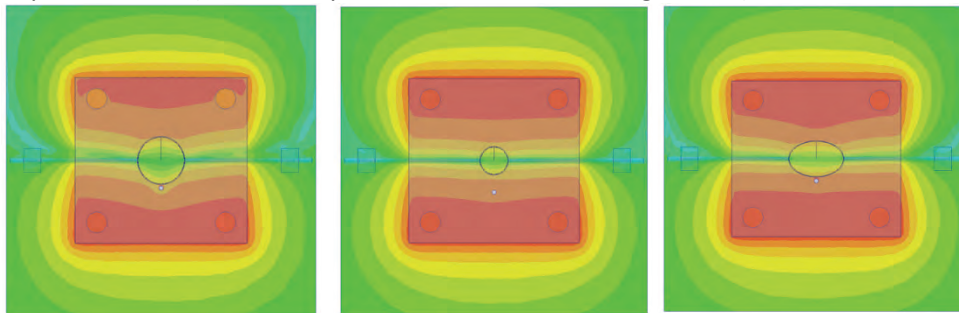


Fig. 43 Subset of 'pumptenna' simulations which were used to investigate different peristaltic cavity configurations; all channels and reservoirs have dielectric fluid with $\epsilon_r = 8$.

An updated CAD model of the prototype is shown on the right side of Fig. 44; this shows the central channel running laterally beneath the patch, the central reservoir which resides at the center of the rectangular patch structure, and dielectric supports for the fluid channel and platform for the metallization of the microstrip patch antenna. The fluidic mechanisms and antenna were co-designed specifically for the purpose of isolating the pumping mechanism from the performance of the antenna (e.g., to be invariant to dielectric loading from the fluidic dispersion and impedance loading from the capacitive displacement of the central deformable region). This was accomplished by removing the metallization from the top of the deformable region (which required slight design modifications to the patch) and placing the fluid line at the location of constant low electric field strength beneath the patch. This provides an opportunity to use this as a multifunctional antenna reconfiguration system, in particular, for the use of a low dielectric fluid ($\epsilon_r = 2$) in thermoregulation operation and the use of a

high dielectric fluid ($\epsilon_r = 16$) for antenna reconfiguration operations. The electric field distribution beneath the metalized patch for both cases has been included on the left side of Fig. 44. These are nearly identical, which provides some visual evidence that the deformable pumping mechanism and fluidic feed lines do not alter the performance governing field distributions in these two cases.

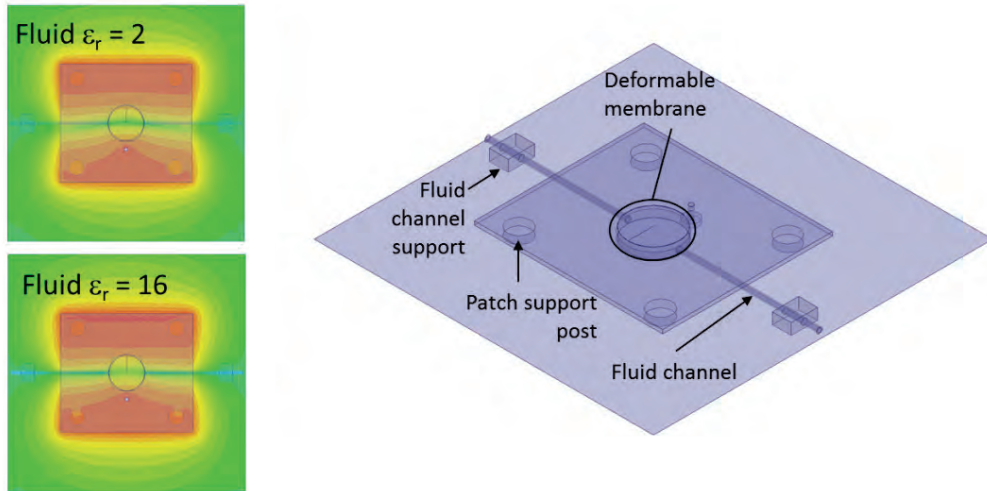


Fig. 44 Subset of 'pumptenna' simulations which were used to investigate different material properties in the antenna; (right) the CAD model of the second revision of the 'pumptenna'.

The simulated VSWR and radiation patterns at 2.6 GHz have been included for the low and high dielectric fluids in Fig. 45 and Fig. 46, respectively, to provide a more in-depth view of the antenna's electromagnetic performance as the top of the deformable region is displaced vertically from flat up to a 0.6 mm displacement at the center of the deformable membrane. This demonstrates that there is some shifting of the matched impedance bandwidth as the antenna pumps, but this design issue is minor and can be removed from the design of the structure. These results indicate that the antenna is operating as intended (with minor exceptions).

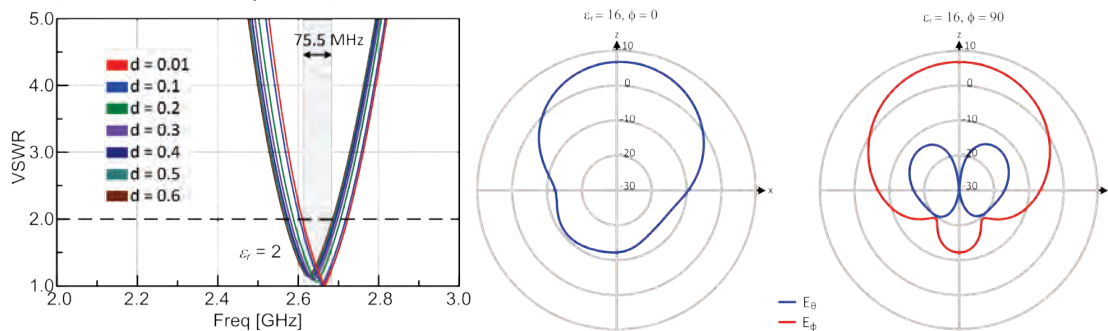


Fig. 45 Simulated VSWR as a function of deformable membrane displacement (left) and radiation patterns at 2.6 GHz for the case when a low dielectric fluid resides in the fluidic system.

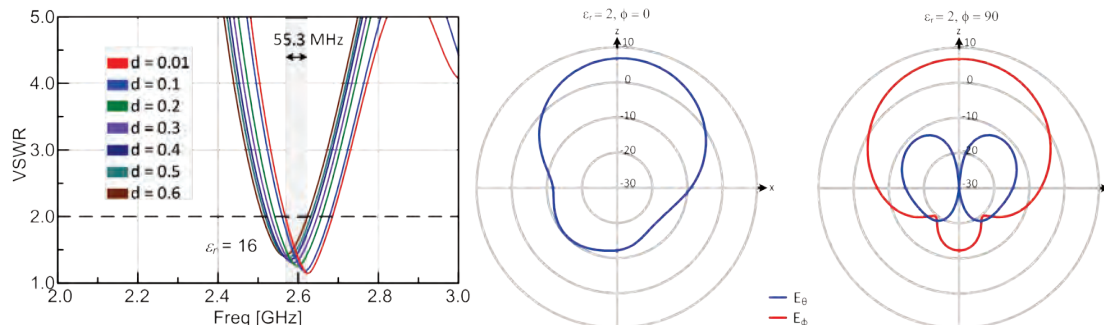


Fig. 46 Simulated VSWR as a function of deformable membrane displacement (left) and radiation patterns at 2.6 GHz for the case when a low dielectric fluid resides in the fluidic system.

ii. Develop automated test bench to analyze adaptive capabilities of reconfigurable antennas

A major component of this research goal was integrated into the reconfigurable antenna system in Fig. 38, but other activities relevant to this were performed in this project. This includes a novel system that was constructed as a multi-university senior design project. The goal was to move individual nanoparticles by controlling the voltage applied to pairs of electrodes using the touch screen of an Android tablet with camera feedback. This system can be used for a reconfigurable antenna or as a tool in colloidal system research. The resulting ‘Android Particle Controller’ is composed of a camera, a microcontroller, an electric and magnetic field generation board (EM Board), a server, and an Android application running on a tablet computer. The Android application connects to the server and sends coordinates corresponding to the location of the user’s touch on the touchscreen. The image processing subsystem captures the camera feed and filters the image to locate the particles and determine their coordinates. The image processing subsystem then sends these coordinates to the server. The server computes the difference between the touch and particle coordinates and determines the required voltage levels for the electrodes to move the particle to the location of the user’s touch on the touchscreen. These voltage levels are produced by the microcontroller and applied to the electrodes on the EM control board, which surrounds the manipulation area. Fig. 47 shows the physical layout of the system. All components of the system interact with the server over a wireless network using a router. The wireless signal waves represent an element of the system that sends or receives wireless signals.

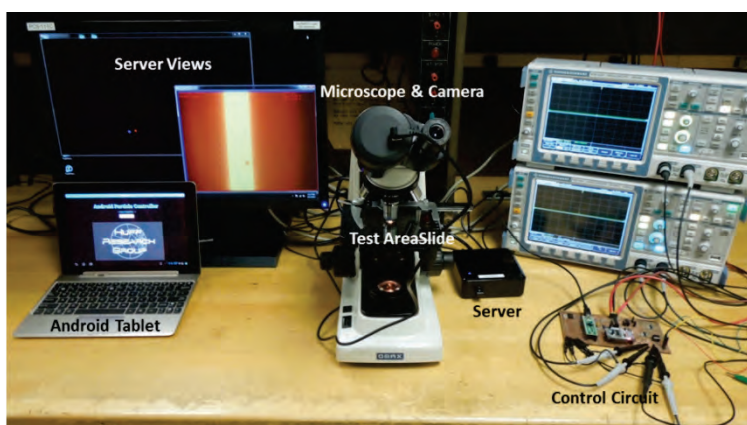


Fig. 47 Physical layout of the Android Particle Controller system.

The system consists of a microscope camera that is focused on a set of electrodes (where the nanoparticles are at rest). The camera attached to the microscope captures images of the setup which are processed in order to determine the locations of the particles. The user interacts with the android

application which sends data to the server. The server computes the required voltages based on the user input and particle locations and sends the values to the control circuit. The control circuit produces the voltage signals which are applied to pairs of electrodes. The voltage difference across the electrodes creates an electric field which moves the particles. Fig. 49 shows the final system setup on the Android tablet and Fig. 49 shows the user screen during operation. The system allows two modes of operation, a DC mode and an AC mode. The DC mode uses the coordinates of the user's touch and the coordinates of a single particle to produce DC voltages on the electrodes which guide the particle towards the user's touch. The AC mode allows the user to run sinusoidal amplitude sweeps across the electrodes and monitor the behavior of the particles. The system records the locations of all of the particles in the image as the sweep runs. This data can be processed in order to study particle behavior in response to a variety of applied electric fields.

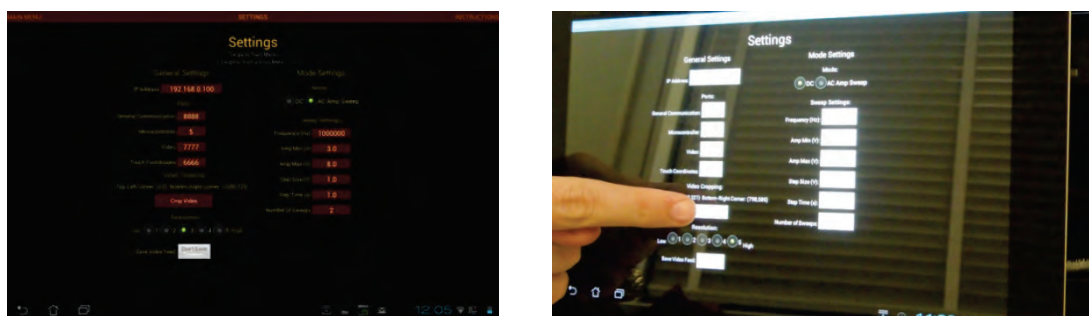


Fig. 48 Physical Layout of the System Component

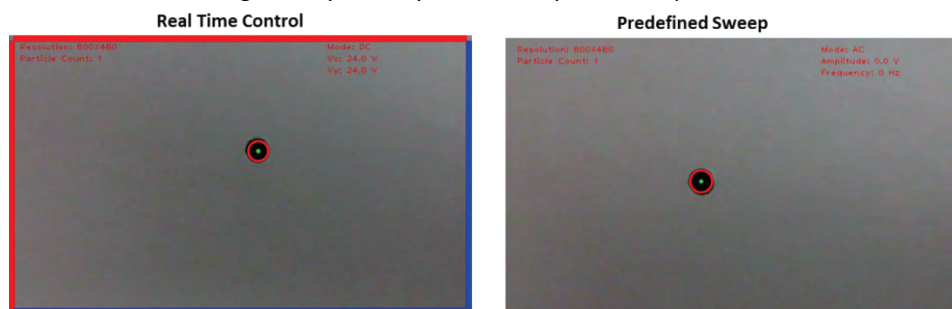


Fig. 49 DC mode Tablet image (left) and AC mode tablet image (right).

C. Summary of Archival Publications and Other Disseminated Work Supported by Grant

i. Archival (Peer Reviewed) Publications

- [1] Multiple Electrokinetic Actuators for Feedback Control of Colloidal Crystal Size, Juarez, J.J.; Mathaib, P.P.; Liddle, J.A.; Bevan, M.A. Lab Chip Vol.12, 4063 - 4070, 2012
- [2] Feedback Controlled Colloidal Self-Assembly, Juarez, J.J.; Bevan, M.A. Adv. Funct. Mater. Vol.22, 3833–3839, 2012.
- [3] Analysis of a Variable SIW Resonator Enabled by Dielectric Material Perturbations and Applications, Barrera, J.D. ; Huff, G.H., IEEE Trans. Microw. Theory Techniques. Vol. 61, 225-233, 2013.
- [4] M. Kelley, C. Koo, H. McQuilken, B. Lawrence, S. Li, A. Han, and G. H. Huff, "Frequency reconfigurable patch antenna using liquid metal as switching mechanism," IET Electron. Lett., Vol. 49, No. 22, pp. 1370-1371, Oct. 2013.

ii. Invited Talks, Workshops, and Seminars

- [1] Feedback Controlled Colloidal Self-Assembly, Workshop on Programmable Functional Materials, University of Illinois at Urbana-Champaign, 05.23.2012.
- [2] Feedback Controlled Colloidal Self-Assembly, CECAM workshop on Emergent Dynamics in Driven Colloids, Lausanne, Switzerland, 04.27.2012.

iii. Conference, Symposia, and Other Activities

- [1] G. H. Huff, J. D. Barrera, S. A. Long, "Multi-scale modeling of antenna reconfiguration mechanisms based on fluidic dispersions of nanoparticles," *pres. at IEEE Int. Symp. on Antennas and Propag. and USNC/URSI Nat. Radio Sci. Mtg.*, Chicago, IL, Jul. 2012.
- [2] F. J. Drummond, M. Young, and G. H. Huff, "Material enhancement strategies and CFD analysis of an aerodynamically functionalized antenna," *pres. at IEEE Int. Symp. on Antennas and Propag. and USNC/URSI Nat. Radio Sci. Mtg.*, Orlando, FL, Jul. 2013.
- [3] H. McQuilken, B. Lawrence, R. Silva, M. Kelley, S. Li, C. Koo, A. Han, and G. H. Huff, "Fluidic tuning of a microstrip patch antenna for ISM and GPS bands," *pres. at IEEE Int. Symp. on Antennas and Propag. and USNC/URSI Nat. Radio Sci. Mtg.*, Orlando, FL, Jul. 2013.
- [4] M. Kelley and G. H. Huff, "Fluidic tuning of a frequency selective surface based on a four-arm Archimedean spiral," *pres. at IEEE Int. Symp. on Antennas and Propag. and USNC/URSI Nat. Radio Sci. Mtg.*, Orlando, FL, Jul. 2013.

iv. Awards, Accolades, and Other Recognition

- [1] Featured Author and Featured Article, EIT Electron. Lett., 2013 (for "Frequency reconfigurable patch antenna using liquid metal as switching mechanism")

D. Extensions Granted or Milestones Slipped (if any)

A no-cost extension was requested and granted in this project. This was a six (6) month extension requested to extend the original closing date of 31-MAR-2015 to a proposed closing date of 30-SEP-2015. This extension (01-APR-2015 to 30-SEP-2015) was requested to be able to complete the scope of work proposed in the project, and to complete mentoring activities in the Spring 2015 and Summer 2015 academic semesters for undergraduate, graduate, and post-doctoral personnel supported by this project who will contribute to advanced technical areas in the US workforce through the training provided by this project.

E. Changes in Research Objectives (if any)

There are no major changes in research objectives to report.

F. Change in AFOSR Program Manager (if any)

There are no major changes in AFOSR program manager to report.

1.

1. Report Type

Final Report

Primary Contact E-mail**Contact email if there is a problem with the report.**

prof.ghuff@gmail.com

Primary Contact Phone Number**Contact phone number if there is a problem with the report**

21755235668

Organization / Institution name

Texas A&M University

Grant/Contract Title**The full title of the funded effort.**

Multifunctional Material Systems for Reconfigurable Antennas in Superconfigurable Structures

Grant/Contract Number**AFOSR assigned control number. It must begin with "FA9550" or "F49620" or "FA2386".**

FA9550-12-1-0090

Principal Investigator Name**The full name of the principal investigator on the grant or contract.**

Gregory H. Huff

Program Manager**The AFOSR Program Manager currently assigned to the award**

Byung-Lip Lee

Reporting Period Start Date

04/01/2012

Reporting Period End Date

09/30/2015

Abstract

The overarching goal of this project is to pursue multidisciplinary engineering research objectives related to the analysis, design, operation, and integration of superconfigurable antenna systems enabled by fluidic dispersions of nanoparticles and multifunctional composites. A multi-scale approach focusing on a range of carefully targeted experimental observations, numerical simulations, and analytical modeling techniques are being used to accomplish the individual tasks associated with this objective. This broadly-defined scope of activities also serves as a connective mechanism between fundamental physical behavior and intrinsic properties to paradigms for dynamic control at the particle level to engineering design concepts and application spaces. Several system-level demonstration vehicles are examined in this process, which are intended to act as a pathway for the transition of these advancements into relevant technologies. Activities in this project include the fabrication and evaluation of new fluidic-based material systems, integrative and adaptive control techniques, and the application of these dynamic systems to engineer novel superconfigurable antenna systems. This includes reconfiguration mechanisms (switches, reactive loads, and filters) and reconfigurable antennas (resonant and traveling wave) are being developed to study the interaction of these materials systems at the application-scale to facilitate changes in frequency selectivity, directional radiation characteristics, and thermal behavior in an automated deformable antenna test-bed. Microstrip and stripline topologies will be focused on for this project to ensure interoperability of

new technologies since these topologies are readily integrated into existing systems. These will be engineered around the common operational objective of enabling advanced sensing (radar) and wireless (communication) technologies in a collection of frequency bands of strategic interest to the Air Force and other DoD branches. This will include UHF (0.3-3 GHz), S-Band (2-4 GHz), and X-band (8-12 GHz), but analysis and experimentation will be performed on high performing technologies up to the PI's instrumentation limit of 70 GHz (into V-band) to explore emerging design spaces.

Distribution Statement

This is block 12 on the SF298 form.

Distribution A - Approved for Public Release

Explanation for Distribution Statement

If this is not approved for public release, please provide a short explanation. E.g., contains proprietary information.

SF298 Form

Please attach your [SF298](#) form. A blank SF298 can be found [here](#). Please do not password protect or secure the PDF. The maximum file size for an SF298 is 50MB.

[SF298-FA9550-12-1-0090.pdf](#)

Upload the Report Document. File must be a PDF. Please do not password protect or secure the PDF. The maximum file size for the Report Document is 50MB.

[Final Performance Report for FAFA9550-12-1-0090 \[TAMU JHU PSU\].pdf](#)

Upload a Report Document, if any. The maximum file size for the Report Document is 50MB.

Archival Publications (published) during reporting period:

See attached document.

Changes in research objectives (if any):

None.

Change in AFOSR Program Manager, if any:

None.

Extensions granted or milestones slipped, if any:

None.

AFOSR LRIR Number

LRIR Title

Reporting Period

Laboratory Task Manager

Program Officer

Research Objectives

Technical Summary

Funding Summary by Cost Category (by FY, \$K)

	Starting FY	FY+1	FY+2
Salary			
Equipment/Facilities			
Supplies			
Total			

Report Document

Report Document - Text Analysis

Report Document - Text Analysis

Appendix Documents

2. Thank You

E-mail user

Dec 21, 2015 11:55:00 Success: Email Sent to: prof.ghuff@gmail.com